[redacted]

CONFIDENTIAL

Copy
RM L56K22

NACA

RESEARCH MEMORANDUM

DRAG OF CONICAL AND CIRCULAR-ARC BOATTAIL AFTERBODIES AT MACH NUMBERS FROM 0.6 TO 1.3

By Frank V. Silhan and James M. Cubbage, Jr.

Langley Aeronautical Laboratory
Langley Field, Va.

NATIONAL ADVISORY COMMITTEE
FOR AERONAUTICS

WASHINGTON

January 22, 1957

CONFIDENTIAL

[redacted]

R

NACA RM L56K22

[redacted]

NATIONAL ADVISORY COMMITTEE FOR AERONAUTICS

RESEARCH MEMORANDUM

DRAG OF CONICAL AND CIRCULAR-ARC BOATTAIL AFTERBODIES AT MACH NUMBERS FROM 0.6 TO 1.3

By Frank V. Silhan and James M. Cubbage, Jr.

SUMMARY

Drag characteristics of a series of related conical and circular-arc afterbodies are presented for Mach numbers from 0.6 to 1.3. Drag was obtained from pressure measurements on the boattail and solid base. The boattail angles tested ranged from 0° to 45° for ratios of base diameter to maximum body diameter ranging from 0 to 1.0.

The results of the investigation indicate that increasing the ratio of base diameter to maximum diameter beyond 0.55 is, in general, detrimental from a drag standpoint. The minimum-drag boattail angle for conical afterbodies at a Mach number of 0.9 and all diameter ratios tested was approximately 7° and for circular-arc afterbodies approximately 16°; at a Mach number of 1.2, the data indicate optima of approximately 4° for the cones and 7° for the circular arcs. On the basis of equivalent fineness ratio and ratio of base diameter to maximum diameter the circular-arc afterbodies gave lower boattail drag than conical afterbodies for conical boattail angles greater than approximately 8° (16° circular-arc boattail angle), but for angles less than 8° the boattail drag for the cones was slightly lower. For total drag, similar results were obtained except for a reduction of the difference between the two types of boattailing for cone angles less than 8°.

INTRODUCTION

At transonic and supersonic speeds a significant part of the total drag of aircraft or missiles is associated with reduced pressures along the afterbody of the fuselage or nacelles. The problem of designing an afterbody to fair from a fixed diameter of a fuselage or nacelle to a fixed diameter of the base so that minimum drag would be obtained for both supersonic and subsonic flight has received considerable attention. Calculation of afterbody drag can be readily accomplished at supersonic speeds and the literature contains numerous experimental investigations

[redacted]

[redacted]

at these speeds. At the higher subsonic speeds of current interest for cruise operation, theoretical determination of the drag is not readily accomplished, and at low supersonic speeds the theory is restricted to thin bodies. Experimental data at transonic speeds are reported in references 1 to 6 and elsewhere, but for the most part consist of results from specific configurations or from afterbodies with stabilizing fins.

The investigation reported herein is part of a general program in progress in the Internal Aerodynamics Branch of the Langley Compressibility Research Division to study the drag of afterbodies through the transonic range. The present work concerns the drag of a series of conical and circular-arc afterbodies without an issuing jet. The boattail angle of the conical and circular-arc afterbodies tested ranged from 0° to 45° and the ratio of base diameter to maximum diameter varied from 0 to 1.0. These 1-inch-diameter afterbodies were attached to a cylindrical sting which extended upstream into the tunnel entrance bell. The tunnel test section was slotted and data were obtained over a Mach number range from 0.6 to 1.3. The corresponding Reynolds number range was 3.3×10^6 to 4.4×10^6 per foot.

SYMBOLS

A	area
d	diameter
C_D	total-drag coefficient, boattail plus base, $C_{D,\beta} + C_{D,b}$
$C_{D,\beta}$	boattail-drag coefficient, $\int_1^{(r_b/r_m)^2} C_p \, d\left(\frac{r_x}{r_m}\right)^2$
$C_{D,b}$	base-drag coefficient, $-C_{p,b} \frac{A_b}{A_m}$
C_p	pressure coefficient, $\frac{p_x - p_\infty}{q_\infty}$
H	total pressure
l	length of boattail
M	stream Mach number
p	static pressure

q dynamic pressure, $\rho V^2/2$

r radius

V velocity

x distance downstream from point of initial decrease from diameter of 1 inch (for cylindrical afterbody only, x is measured from a point 2 maximum body diameters upstream of base)

y radial distance from surface

β boattail angle between center line of model and tangent line at base of model

ρ mass density

Subscripts:

β boattail

b base

x local

m maximum

∞ stream conditions

APPARATUS AND METHODS

A photograph showing the general arrangement of the experimental setup used in this investigation is presented in figure 1. The top and bottom walls of the $4\frac{1}{2}$-inch-square slotted test section contained four slots each; the width of the slots was such that the ratio of open area to total area of each slotted wall was 1/8. The afterbody models were attached to a 1-inch-diameter sting supported along the tunnel center line by the system of struts shown in figure 1. Air at a maximum stagnation pressure of 2 atmospheres was supplied by a centrifugal compressor; auxiliary suction was applied to the plenum chamber surrounding the test section to obtain supersonic Mach numbers. The test-section-empty Mach number distributions and construction details of this tunnel are presented in reference 7. For the range of Mach numbers near 1, tunnel-wall effects cause some uncertainty in the data. At the higher Mach numbers of the investigation, however, reflected disturbances which originate on the

boattail fall well downstream of the base for all but a few of the longest models. For the longest of these the reflected disturbances are just rearward of the body at the highest Mach number. Although the magnitude of any wall effect present is unknown, it is felt, from previous experience and checks with other data where possible, that these effects are relatively small and that the data trends established are valid throughout the speed range of these tests.

Two types of afterbody contours were tested in this investigation: conical and circular-arc contours. Photographs of several models are presented in figure 2; sketches are also shown in figure 3 together with tables summarizing pertinent dimensions and the number of pressure orifices of each model tested. Boattail angles of 0°, 3°, 5.6°, 8°, 16°, and 45° were tested; ratios of base diameter to maximum body diameter were 0, 0.55, 0.70, 0.85, and 1.0. Radii for the profiles of the circular-arc afterbodies were chosen so that the tangent to the arc at the base formed the desired boattail angle. Afterbody models with low boattail angles and small-diameter ratios were not tested due to their extreme length. Pressure measurements were obtained from a number of orifices installed in a helical path around the afterbody and on the model base. The number of orifices in a particular model varied according to the length of the model. For models containing more than one base-pressure orifice, an average of the base pressures was used in determining base drag. The free-stream static-pressure orifice was located on the sting approximately 1 body diameter upstream of the cylinder-afterbody juncture.

A boundary-layer survey was made to estimate the depth and profile of the boundary layer approaching the afterbody. The survey model had six total-pressure probes, 0.030 inch in diameter, equally spaced about the circumference at varying heights from the surface and in the plane corresponding to the sting-boattail juncture. The ends of the probes were flattened to give an opening approximately 0.006 inch in height. Velocity profiles obtained at three stream Mach numbers are presented in figure 4 together with a 1/7-power profile. The profiles show a thick turbulent boundary layer approaching the afterbody. The effect of boundary-layer thickness was not investigated although it may change the level of the curves. However, it is felt that the relative drag of the different models would not change with boundary-layer thickness. This is borne out in the investigations of references 5 and 8 which include the effect of varying boundary-layer thickness for afterbodies with jet flow. Both show only a small effect due to increases in boundary-layer thickness from 0.095 to 0.184 of the maximum body diameter at transonic speeds and at $M = 1.5$ (ref. 5) and from 0.05 to 0.18 at $M = 1.9$ (ref. 8). Extrapolation to the no-jet-flow condition of the data of reference 8 ($C_{p,b}$ as a function of jet pressure ratio) indicates a change in $C_{p,b}$ of approximately 4 percent.

Afterbody pressures were recorded at Mach numbers from 0.6 to about 1.3. At each test point, all pressures were photographically recorded from a mercury-filled, multitube manometer. The measured pressure distributions were mechanically integrated to obtain the pressure drag. Schlieren photographs of the flow were also taken at a majority of the test conditions. The Reynolds number range of these tests was 3.3×10^6 to 4.4×10^6 per foot.

RESULTS AND DISCUSSIONS

Afterbody Pressure Distributions

Pressures measured along several of the conical and circular-arc afterbodies studied in this investigation are presented in coefficient form as a function of the distance along the afterbody in figures 5 and 6. Schlieren photographs of the flow field about the afterbody for several of the afterbody models are also shown in figures 5 and 6.

Figure 5 shows the changes that occur in the pressure distributions over conical and circular-arc afterbodies with boattail angles of 5.6° and 16° as the stream Mach number varies from 0.6 to 1.3. The pressure distributions over the 5.6° conical afterbody (fig. 5(a)) are typical of those over other low-angle cones. The abrupt expansion of the flow at the cone-cylinder juncture at $M \geqq 1.0$ is in good agreement with that calculated for a Prandtl-Meyer turn equal to the boattail angle β. (The latter value is indicated by the arrow on the ordinate at $x/d_m = 0$.) Compression of the flow over the afterbody at subsonic Mach numbers is more rapid than the supersonic compression. For the shortest afterbody, $d_b/d_m = 0.85$, the pressure coefficient decreased abruptly ahead of the base due to the influence of the base pressure. The initial expansion and pressures upstream of the base were nearly independent of the ratio of base diameter to maximum diameter. The continued compression of the flow over a longer afterbody ($d_b/d_m = 0.55$) was sufficient to produce positive values of $C_{p,\beta}$ at $M = 0.9$ and 1.0. The influence of the base pressure extended somewhat farther forward as the afterbody length increased. Although the extent of the initial expansion and subsequent compression was greater at $\beta = 16°$ (fig. 5(b)) the effects of Mach number and ratio of base diameter to maximum diameter were essentially the same as at the lower boattail angles. The values of $C_{p,\beta}$ calculated for a Prandtl-Meyer expansion of 16° is not in as good agreement with the measured pressure as it was for the $\beta = 5.6°$ model.

The schlieren photographs of figures 5(a) and (b) show the difference in the flow over a 5.6° and 16° boattailed afterbody. The absence

of a trailing shock on the 5.6° afterbody will be noted in figure 5(a) at all speeds due to the gradual recompression of the flow along the afterbody following the initial expansion to 5.6°. Along the 16° model (fig. 5(b)), however, the recompression occurs in a much shorter distance, and the flow, unable to negotiate this higher gradient, separates from the body to produce the trailing shock observed in the photographs. As the Mach number increases, this trailing shock moves rearward on the model until at $M = 1.3$ it is located close to the base.

For the circular-arc-profile afterbodies (figs. 5(c) and (d)) the pressure just downstream of the point of tangency was well below the freestream static pressure in some instances (fig. 5(d)). This must be attributed largely to the thinning of the boundary layer ahead of the tangency point and subsequent acceleration of the flow. For a long, low-angle afterbody $d_b/d_m = 0.70$ (fig. 5(c)) the pressure coefficient along the afterbody was nearly constant at all Mach numbers. Along the shortest afterbody, $d_b/d_m = 0.85$, the pressure tended to decrease to a minimum at $x/d_m \approx 1$ and then remains essentially constant. For $\beta = 16°$ (fig. 5(d)) the decrease to minimum pressure was quite rapid as was the subsequent increase in pressure. The point of minimum pressure moved rearward on the afterbody as M increased and as the afterbody became longer (decreasing d_b/d_m). Positive pressures occurred on the rear part of the afterbody for the $\beta = 16°$, $d_b/d_m = 0.55$ model from $M = 0.6$ to 1.0. The schlieren photographs indicate no separation of the flow over the low-angle body (fig. 5(c)), and limited separation affected only a small portion of the 16° afterbody (fig. 5(d)).

Figure 6 shows the variation in the pressure-coefficient distributions over the afterbody for different values of boattail angle at a constant value of d_b/d_m. The distributions shown for $\beta = 0°$ (cylindrical afterbody) were obtained from reference 3. Since the pressure drag of a cylindrical afterbody is represented entirely by the base drag, the area under the curve for $\beta = 0°$ in figure 6 does not represent a pressure drag force. The schlieren photographs and pressure distributions for the conical afterbody with $\beta = 45°$ show the flow to be separated over the entire length of the afterbody. Unpublished data obtained by the Internal Aerodynamics Branch for a 30° afterbody show that the flow completely separates at this value of β also. The distributions for $\beta = 8°$ and 16° at $M = 1.1$ are not consistent with the trend of the distributions for other Mach numbers perhaps as a result of an error in the static-pressure measurement. As indicated in figure 3(b), these models had only three static orifices available to determine the pressure distributions.

For the circular-arc models (fig. 6(b)) the boattail angle had only a small effect on the distributions up to $\beta = 8°$. The difference between the shape of the distributions for $\beta = 5.6°$ and $\beta = 8°$ was

more pronounced at supersonic speeds than at subsonic speeds. The flow over the $\beta = 45^\circ$ model remained attached to the model for a short distance downstream of the tangency point causing the flow to expand to low pressures in this region.

Afterbody Drag

Preliminary tests were conducted on a cylindrical afterbody for comparison with data from other sources; the results are presented in figure 7 as a function of free-stream Mach number. The cylindrical model was selected because there is a substantial amount of transonic data from wind-tunnel and flight tests available for comparison. The wind-tunnel data presented were obtained from similar configurations, an infinitely long forebody with a relatively thick turbulent boundary layer. The flight model (ref. 2), of fineness ratio 11, contained a large cavity in the base and the drag coefficient presented is the sum of the drag coefficients over the center base area and the annulus area. The drag variation with stream Mach number is, in general, similar for the four sets of results presented although the numerical values show significant percentage differences. The exact cause of these differences has not been ascertained; possible factors are wind-tunnel-wall interference, model boundary layer, or Reynolds number.

Basic data.- The basic drag data are presented in figure 8 for all configurations tested. The boattail-drag coefficient $C_{D,\beta}$, base-drag coefficient $C_{D,b}$, and the total-afterbody-drag coefficient C_D are presented as functions of the free-stream Mach number for constant values of β and d_b/d_m. The data obtained in tests of conical models are presented in figures 8(a) to (e); those from circular-arc-model tests in figures 8(f) to (j).

For the 3° conical afterbody, changes in Mach number had little effect on the boattail-drag coefficient. The subsonic drag coefficient was low, approximately 0.025, with only a small transonic rise. Extending the afterbody and thus reducing the ratio of base diameter to maximum diameter led to small increases in the boattail drag at supersonic speeds but effected large reductions in the base drag. Because the base drag is substantially greater than the boattail drag, the total drag was smaller for the longer body.

At a boattail angle of 5.6° the boattail drag at subsonic speeds was essentially independent of the base diameter, whereas at $M > 1$ substantial increases in $C_{D,\beta}$ accompanied increases in afterbody length. The base drag was somewhat less than the boattail drag for the 5.6° cone at diameter ratios of 0.55 and 0.70, and decreased slightly as the Mach number increased from 0.6 to approximately 1. This same trend

occurs for 3° and 8° cones and for the circular-arc bodies. The reflex in the drag rise of the total-drag plots and the broad Mach number range over which the rise occurs are due to the displacements of the rise in $C_{D,\beta}$ and $C_{D,b}$.

With further increases of β to 8° and 16°, the subsonic level of the boattail drag and the transonic-drag rise continued to increase. The base-drag level decreases for all Mach numbers with a thrust force measured for several configurations. As at the lower angles, the base drag increases with increasing diameter ratio throughout the Mach number range. Models with $d_b/d_m = 0.85$ also gave lower base drag as β increased, but differed from the other diameter ratios in that the base drag at supersonic speeds was always greater than the boattail drag. The base drag agrees well with results of free-flight tests of a $7\frac{1}{2}°$ conical boattail with $d_b/d_m = 0.529$ (ref. 6) as shown in figure 8(c). The free-flight model had fins, but their trailing edge was located about 1 base diameter upstream of the base.

Separation at the cone-cylinder juncture was shown in figure 6(a) to occur when the boattail angle was increased to 45°. The effect of the separation on drag is shown in figure 8(e); the boattail and base drag coefficients vary with the ratio of base diameter to maximum diameter as direct functions of area, while the total drag is essentially independent of diameter ratio.

The boattail drag of the 8° cone is in good agreement with the theoretical results of reference 9 for ratios of base diameter to maximum diameter of 0.55 and 0.70. In general, for smaller boattail angles, the experimental data indicated higher drag with a more rapid decrease with increasing Mach number. Larger boattail angles generally had lower drag which decreased more slowly with Mach number than predicted by reference 9.

The drag data for circular-arc boattailed bodies are presented in figures 8(f) to (j). In general, the variation of drag with Mach number is similar to that for conical boattailed bodies, the most noticeable difference being the lower transonic rise in boattail drag for the circular-arc afterbodies (except $\beta = 45°$). As for conical boattails, the 3° circular-arc model shows a low level of boattail drag with no Mach number effect and a base-drag level of approximately four times the boattail drag. With increasing boattail angle, boattail drag level and transonic drag rise increase and the base-drag level decreases. The base-drag coefficient also increases with increasing base diameter throughout the Mach number range as with the conical boattailed bodies.

The effect of rounding off the sharp break at the cone-cylinder juncture was investigated with two afterbody models. The radius of

curvature was identical for both and was approximately two times the maximum body diameter followed by 16° cones of $d_b/d_m = 0.55$ and 0.70. Subsonically, the curvature produced a small adverse effect on boattail drag of a 16° cone but decreased the drag by approximately 15 percent for the higher Mach number range. The reduction put the boattail drag of the combination circular-arc—cone model roughly midway between the cone drag and the circular-arc drag for $\beta = 16°$.

Effect of boattail angle.- The boattail- and total-drag coefficients for the conical and circular-arc afterbodies are presented in figures 9 and 10 as functions of the boattail angle. Curves are drawn for each of the four diameter ratios investigated for Mach numbers of 0.6, 0.9, and 1.2. Unpublished data from tests of a series of 30° conical afterbodies indicate that separation occurred at the cone-cylinder juncture resulting in measured drag coefficients approximately equal to those obtained in tests of 45° models; therefore, these curves were faired through the same drag coefficient at $\beta = 30°$ as at $\beta = 45°$, although no data were recorded in the present investigation for values of β between 16° and 45°. Arrows along the abscissa indicate the values of β that were tested.

The boattail drag (fig. 9(a)) increased with boattail angle to $\beta = 16°$ as the pressures near the cone-cylinder juncture decreased with increased flow turning; at $\beta = 45°$ the drag varied from above to below the value at $\beta = 16°$ depending on Mach number and diameter ratio. The pressure distributions of figure 6(a) indicate that the increased suction pressures at the cone-cylinder juncture are partially offset by an increase in pressure recovery with β increases. This pressure recovery, however, decreases with increasing Mach number. At Mach numbers of 0.6 and 0.9 the maximum measured drag for a full boattail occurred for the fully separated 45° cone. As the afterbody was shortened, the region of more positive pressures is removed while the peak suction pressures remain so that separation at the cone-cylinder juncture which eliminates the high suction pressures becomes beneficial. At $M = 1.2$ the fully separated cone had less drag than the 16° cone at all diameter ratios tested.

The total-drag data for cones (fig. 9(b)) again show a peak measured drag at $\beta = 16°$ for all diameter ratios at $M = 1.2$. Subsonically, however, the peak drag occurred as the flow separated from the cone-cylinder juncture. The curves show increasing drag as β is reduced in the low-angle range and demonstrate a tendency to fair to the base-drag coefficient of a cylindrical afterbody ($d_b/d_m = 1.0$), which is plotted at $\beta = 0°$. The inclusion of friction drag, however, would produce an increase in total drag which would be greater for the lower values of β. Due to complete separation from the boattail at $\beta = 45°$, the total-drag coefficient is approximately equal to the base-drag coefficient of a cylinder for all Mach numbers and diameter ratios.

[redacted]

The plots of figure 9(b) show a minimum-total-drag coefficient at $M = 0.6$ for a conical boattail angle of about 13° for each of the four diameter ratios and about 7° at $M = 0.9$. The point of minimum drag appears to be at $\beta = 4^\circ$ for $M = 1.2$, at least for the larger diameter ratios where the low angles were investigated. These optima apply to solid base afterbodies and may vary considerably for afterbodies with jet flow issuing from the base. The optimum β values at $M = 0.6$ and 0.9 are in good agreement with those of reference 1. The optima of reference 1 were independent of l/d_m for fineness ratios of 1 to 4, with the minimum drag always occurring for the body with the smallest d_b/d_m. At $M = 1.2$ a β of approximately 5° was optimum for each fineness ratio of reference 1 while reference 4 presents 4.5° as the optimum conical boattail angle for all diameter ratios.

The circular-arc boattail drag (fig. 10(a)) increased with boattail angle for all conditions except at $M = 0.6$ and for the models having the largest diameter ratios where the drag was slightly higher for $\beta = 16^\circ$ than for $\beta = 45^\circ$. The boattail and total drag of the circular-arc bodies is generally lower than for cones of equal boattail angle and diameter ratio; since for the circular-arc models the boundary-layer buildup prevents turning of the flow to the full value of β. In addition, the location of the low pressures in a region farther aft on the model where the radius is small results in a smaller drag contribution.

The total-drag coefficient for a 45° circular-arc afterbody is equivalent to that of a cylindrical afterbody ($\beta = 0^\circ$) at $M = 1.2$ only. For these bodies cylindrical afterbody drag was exceeded only by the shortest 16° circular-arc afterbody. It is also of interest to note that subsonically the very large base-drag coefficients for small boattail angles result in higher total drag than that measured at $\beta = 45^\circ$. The total-drag plots show a gradual curvature in the range of minimum drag at $M = 0.6$ and 0.9 with low points at about 25° and 16°, respectively. At $M = 1.2$ the value of β for minimum drag is more difficult to estimate since the lower boattail angles were not tested for all diameter ratios. The models with a diameter ratio of 0.85 for which all five boattail angles were tested indicate minimum drag at 5°; at $d_b/d_m = 0.70$ the minimum appears to be at $\beta = 7^\circ$. Flight tests of fin-stabilized models (ref. 4) indicate that for parabolic afterbodies a base angle of 9° will give minimum drag.

Effect of ratio of base diameter to maximum diameter.- The boattail- and total-drag coefficients of conical and circular-arc afterbodies are presented as a function of ratio of base diameter to maximum diameter in figures 11 and 12 for five values of β; again, curves are presented for $M = 0.6$, 0.9, and 1.2.

With increasing base diameter and constant β and Mach number a more negative mean pressure results for boattails on which separation does not

occur due to the loss of pressure recovery which occurs on a full boattail ($d_b/d_m = 0$). This effect is offset by the reduction in boattail projected area so that for diameter ratios of 0 to 0.55 the boattail-drag coefficient remains essentially unchanged. Beyond this point $C_{D,\beta}$ falls off to zero at $d_b/d_m = 1.0$ (cylindrical afterbody). Inclusion of the friction drag, however, would increase the drag for low diameter ratios, particularly for low boattail angles. The boattail drag of the 45° cone varies as a direct function of boattail area as a result of the flow separation previously observed.

Addition of the base drag to the boattail drag of the cones produces a marked change in the trend for diameter ratios greater than 0.55. The total drag increases beyond this point to a maximum at $d_b/d_m = 1$ where the base drag of a cylinder is plotted. Exceptions occur for the 16° cone at $M = 1.2$ for which all diameter ratios had greater drag than a cylinder, and for the 45° cone where complete separation results in approximately constant drag.

The drag of the circular-arc boattail shows trends similar to those observed for cones. The drag level for a given value of β, however, is generally lower for circular-arc profiles. The total drag of the circular-arc models increases with diameter ratio for all except the $\beta = 45^\circ$ model where at $M = 1.2$ the drag was approximately constant. The 8° and 16° circular-arc boattails also indicate a total drag greater than that of a cylinder at $M = 1.2$ for diameter ratios close to 1.

Comparison of conical and circular-arc afterbodies.- Comparisons of the two types of boattailing on the basis of equivalent boattail angle are presented in figure 13. Boattail-drag coefficient is presented as a function of stream Mach number for a ratio of base diameter to maximum diameter of 0.70 and for several values of β. This comparison shows higher boattail drag for conical afterbodies for all conditions except boattail angles lower than about 8° at the subsonic Mach numbers and for the fully separated case (45°) at supersonic speeds.

A comparison based on conical and circular-arc afterbodies of equal length is also presented in figure 13. Data at fineness ratios of 0.5, 1, 2, and 3 were obtained from cross fairing of the basic data curves. For an l/d_m of 0.5 (lower right side of figure) the circular-arc afterbody has lower drag over the entire Mach number range, but with increasing length the difference rapidly decreases until for an l/d_m of 3 the cones demonstrate slightly superior drag performance. These and similar plots for diameter ratios of 0.55 and 0.85 indicate that for equivalent fineness ratios the circular-arc afterbodies give better drag performance than conical boattail angles greater than approximately 8° (circular-arc boattail angles greater than 16°), but for angles less than 8° the conical

afterbodies indicate slightly superior drag performance. Similar results are obtained when the comparison is based on total drag except that for angles less than 8° the small differences offer little to choose between the two types of boattailing.

SUMMARY OF RESULTS

The following results are indicated from an investigation of the effects of boattail angle, base area, and afterbody contour on drag of afterbodies without an issuing jet for Mach numbers of 0.6 to 1.3:

1. At a Mach number of 0.9 the lowest total drag for all diameter ratios tested occurred at a boattail angle of approximately 7° for conical afterbodies; the optimum boattail angle for circular-arc afterbodies was approximately 16°. At a Mach number of 1.2 the optimum boattail angle for the larger diameter ratios was about 4° for conical afterbodies and 7° for circular-arc afterbodies.

2. For a Mach number greater than 1.0 total drag reached a maximum for the 16° cone, exceeding even the drag of a cylindrical afterbody.

3. Increasing the ratio of base diameter to body diameter beyond 0.55 decreased boattail drag but at the expense of large increases in base drag and generally higher total drag.

4. On the basis of equal boattail angle and ratio of base diameter to maximum diameter, the circular-arc afterbodies gave lower boattail-drag coefficients than the conical afterbodies for all conditions except for low boattail angles at subsonic speeds and fully separated flow at supersonic speeds.

5. On the basis of equal fineness ratio and ratio of base diameter to maximum diameter the circular-arc afterbodies gave lower boattail drag than conical afterbodies for conical boattail angles greater than approximately 8° (16° circular-arc boattail angle), but for angles less than 8° the boattail drag for the cones was slightly lower. For total drag, similar results were obtained except for a reduction of the difference between the two types of boattailing for cone angles less than 8°.

Langley Aeronautical Laboratory,
National Advisory Committee for Aeronautics,
Langley Field, Va., November 1, 1956.

[redacted]

REFERENCES

1. Patterson, R. T.: A Wind-Tunnel Investigation of the Drag of Conical Missile Afterbodies at Mach Numbers From 0.40 to 2.47 (TED No. TMB AD-3154). Aero. Rep. 857, David Taylor Model Basin, Navy Dept., Jan. 1954.

2. Hart, Roger G.: Effects of Stabilizing Fins and a Rear-Support Sting on the Base Pressures of a Body of Revolution in Free Flight at Mach Numbers From 0.7 to 1.3. NACA RM L52E06, 1952.

3. Cubbage, James M., Jr.: Jet Effects on Base and Afterbody Pressures of a Cylindrical Afterbody at Transonic Speeds. NACA RM L56C21, 1956.

4. Stoney, William E., Jr.: Some Experimental Effects of Afterbody Shape on the Zero-Lift Drag of Bodies for Mach Numbers Between 0.8 and 1.3. NACA RM L53I01, 1953.

5. Pel, C., and Rustemeyer, A.: Investigation of Turbojet Exhaust-Interference Drag. Rep. R-0801-12, United Aircraft Corp. Res. Dept., Nov. 1955.

6. Falanga, Ralph A.: A Free-Flight Investigation of the Effects of Simulated Sonic Turbojet Exhaust on the Drag of a Boattail Body With Various Jet Sizes From Mach Number 0.87 to 1.50. NACA RM L55F09a, 1955.

7. Nelson, William J., and Cubbage, James M., Jr.: Effects of Slot Location and Geometry on the Flow in a Square Tunnel at Transonic Mach Numbers. NACA RM L53J09, 1953.

8. Cortright, Edgar M., Jr., and Kochendorfer, Fred D.: Jet Effects on Flow Over Afterbodies in Supersonic Stream. NACA RM E53H25, 1953.

9. Fraenkel, L. E.: Curves for Estimating the Wave Drag of Some Bodies of Revolution, Based on Exact and Approximate Theories. C.P. No. 136 (15,685), British A.R.C., 1953.

[redacted]

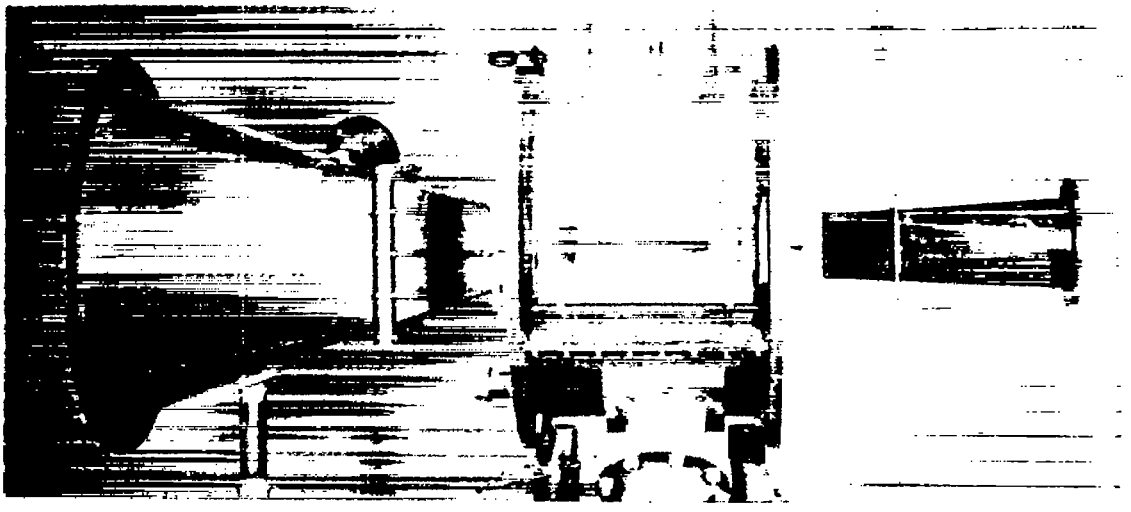

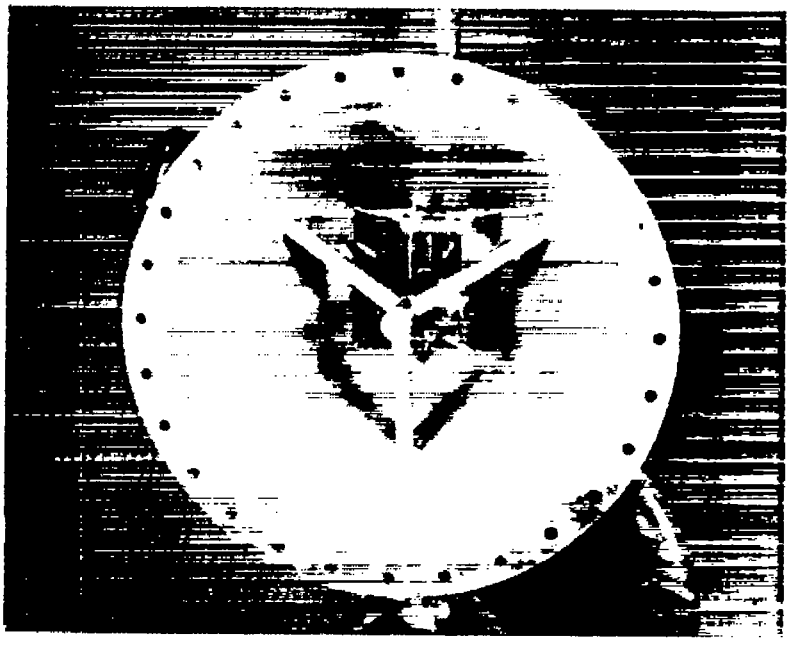

L-95882

Figure 1.- Photograph of slotted channel setup and inlet bell.

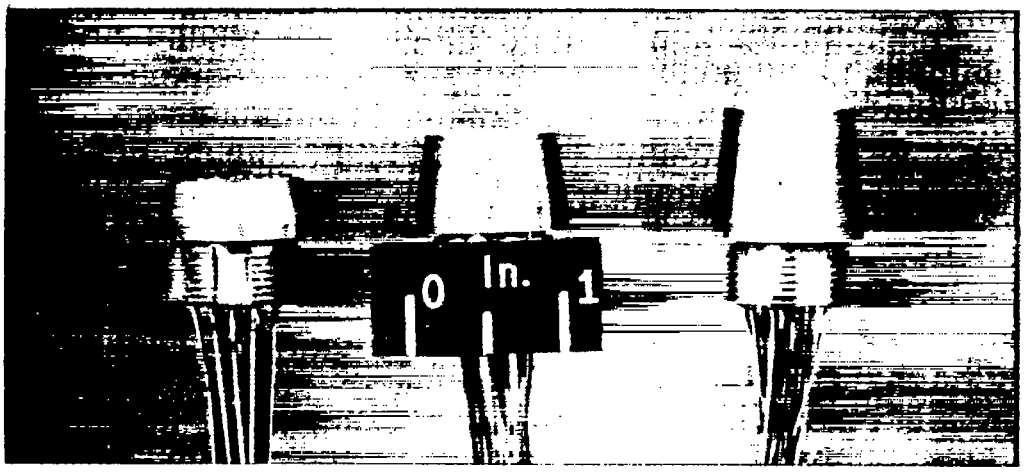

Conical

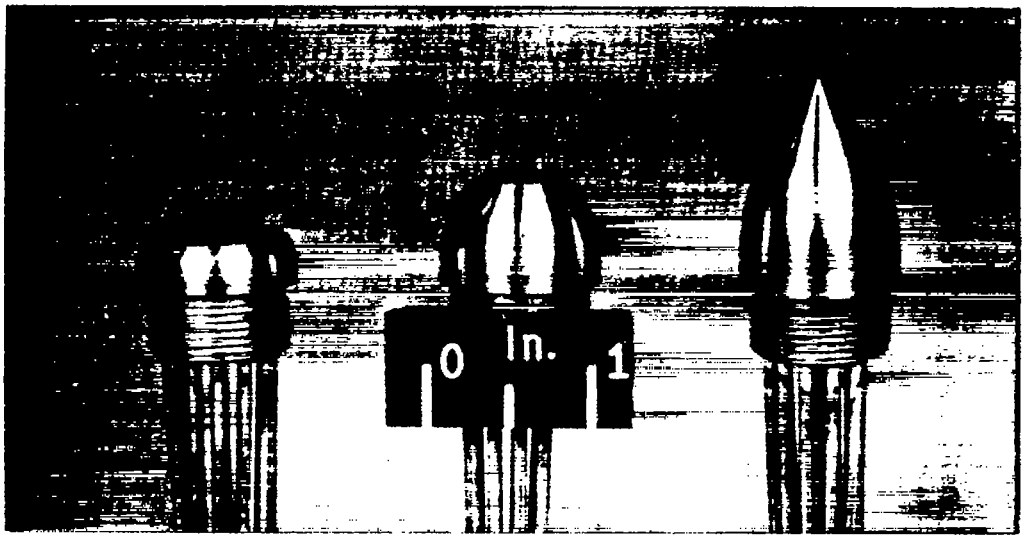

Circular-arc

L-95883

Figure 2.- Photographs of several conical and circular-arc boattail afterbody models.

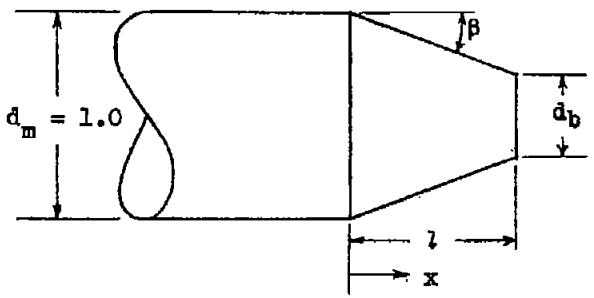

CONICAL AFTERBODIES

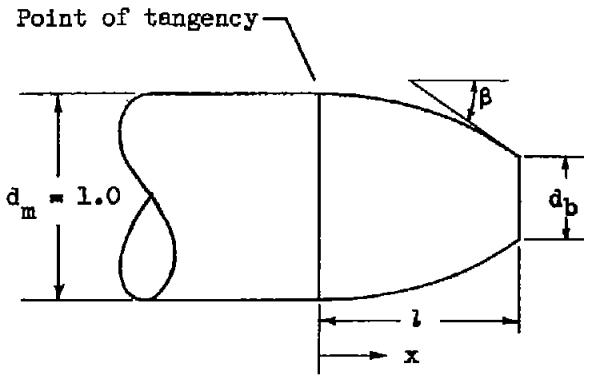

CIRCULAR-ARC AFTERBODIES

Afterbody length, l (all dimensions in inches). Afterbody length, l

d_b/d_m \ β	3°	5.6°	8°	16°	45°
0	—	—	3.56	1.74	.50
.55	—	2.30	1.60	.78	.23
.70	2.86	1.53	1.07	.52	.15
.85	1.43	.77	.53	.26	.08

d_b/d_m \ β	3°	5.6°	8°	16°	45°
0	—	—	—	3.56	1.21
.55	—	—	3.23	1.60	.54
.70	—	3.05	2.15	1.07	.36
.85	2.82	1.53	1.08	.53	.18

(a) Dimensions.

Figure 3.- Dimensions and pressure orifices of the conical and circular-arc boattail afterbodies.

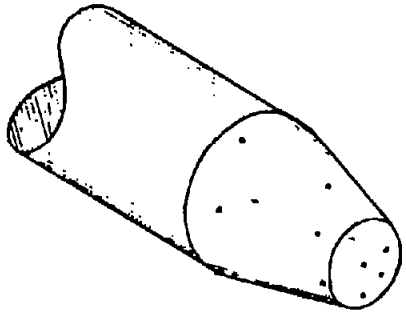

CONICAL AFTERBODIES

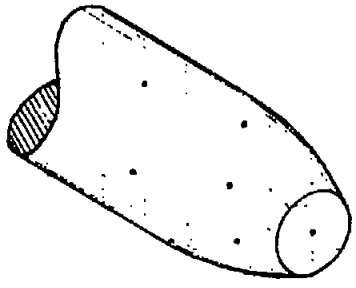

CIRCULAR-ARC AFTERBODIES

d_b/d_m \ β	3°	5.6°	8°	16°	45°
0	—	—	12	12	12
	—	—	0	0	0
.55	—	12	9	9	9
	—	1	3	3	3
.70	12	8	6	6	6
	1	5	6	6	6
.85	6	4	3	3	3
	7	9	9	9	9

← BOATTAIL →
← BASE →

d_b/d_m \ ρ	3°	5.6°	8°	16°	45°
0	—	—	—	11	11
	—	—	—	0	0
.55	—	—	12	12	7
	—	—	1	1	1
.70	—	12	12	12	7
	—	1	1	1	1
.85	12	12	12	7	7
	1	1	1	1	1

(b) Boattail- and base-pressure orifices.

Figure 3.- Concluded.

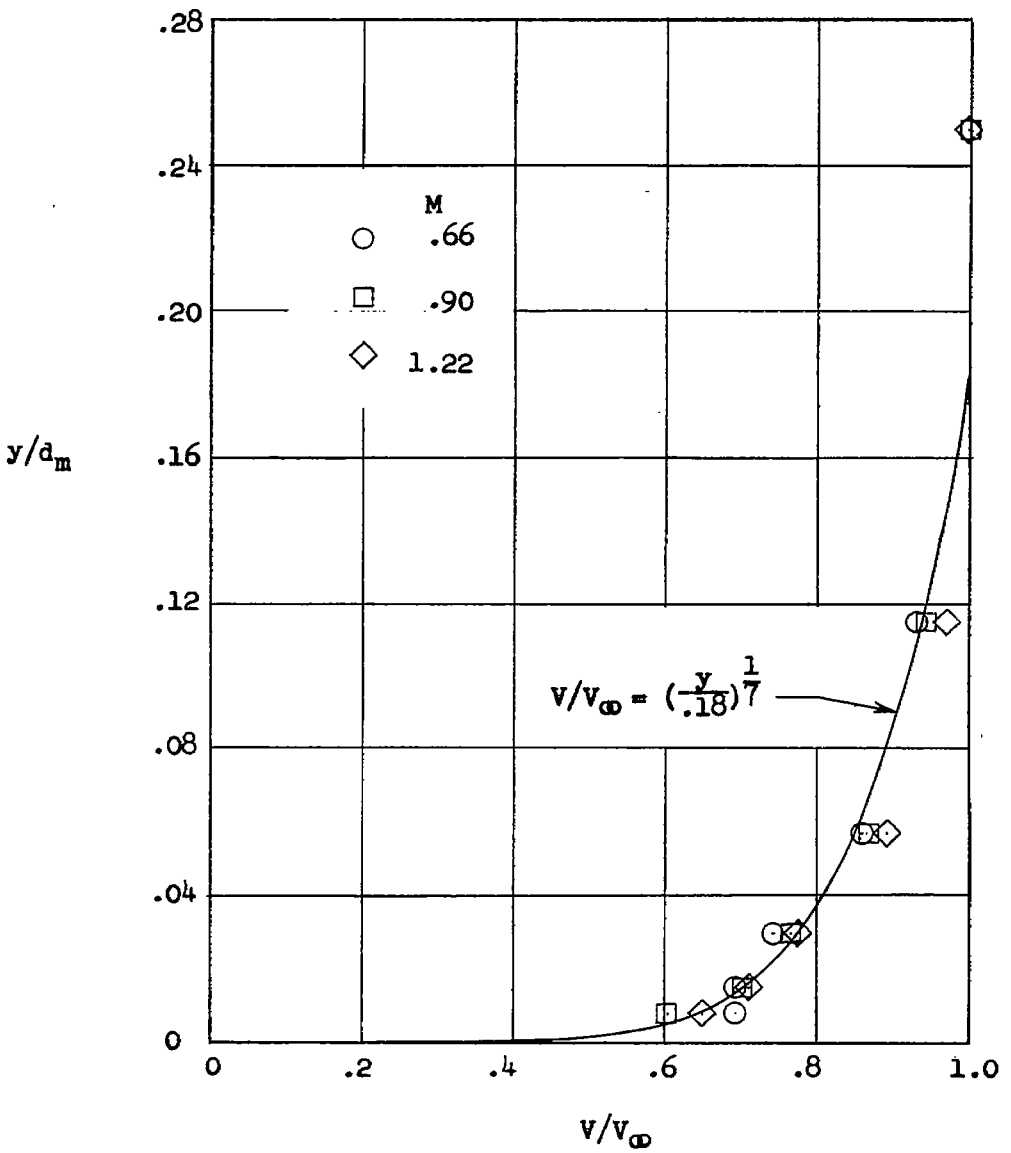

Figure 4.- Velocity profiles at sting-boattail juncture.

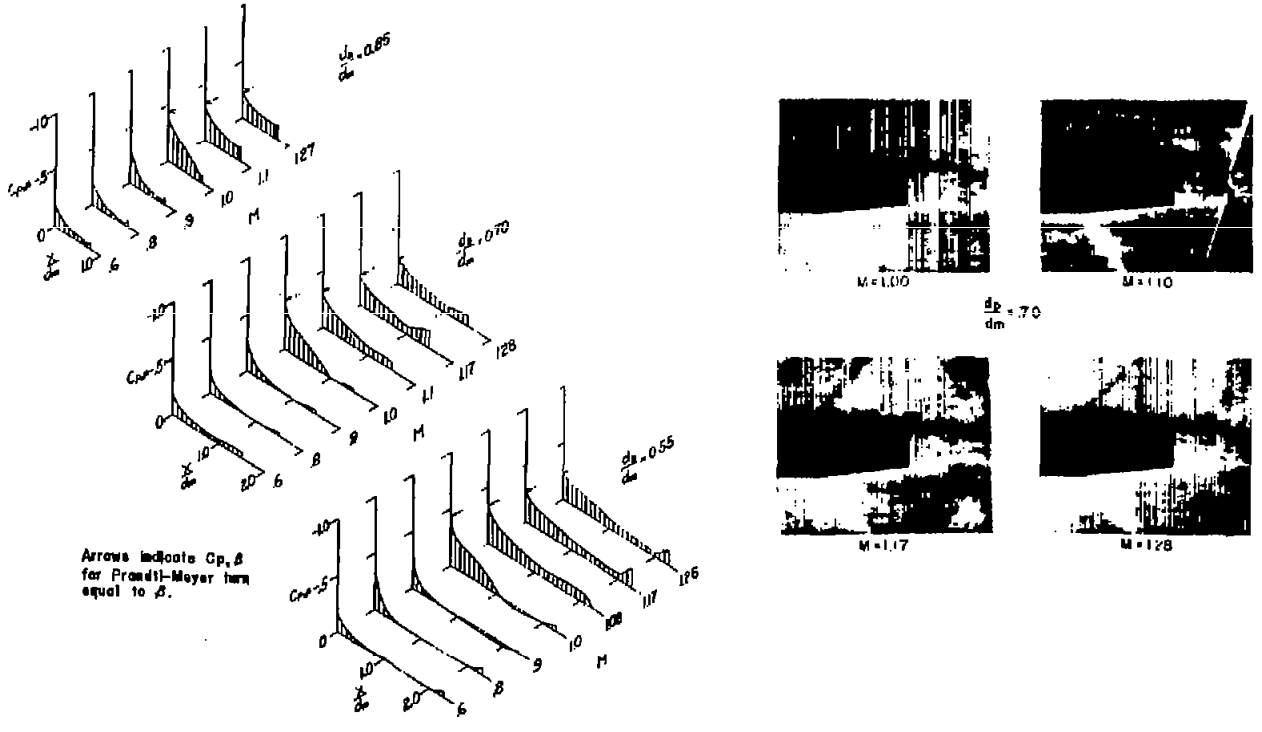

(a) Conical afterbody; $\beta = 5.6^{\circ}$. L-93606.1

Figure 5.- Variation of afterbody pressure coefficient with distance along afterbody for several values of ratio of base diameter to maximum diameter and stream Mach number.

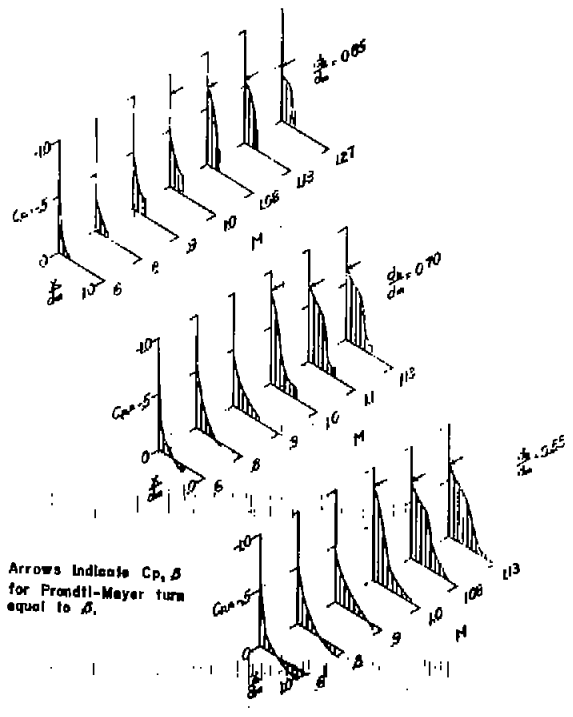

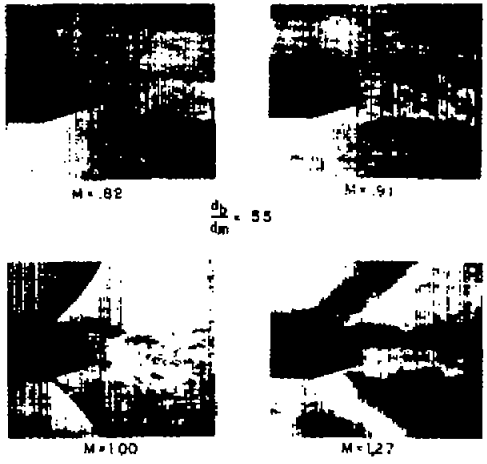

(b) Conical afterbody; $\beta = 16^{\circ}$. L-93605.1

Figure 5.- Continued.

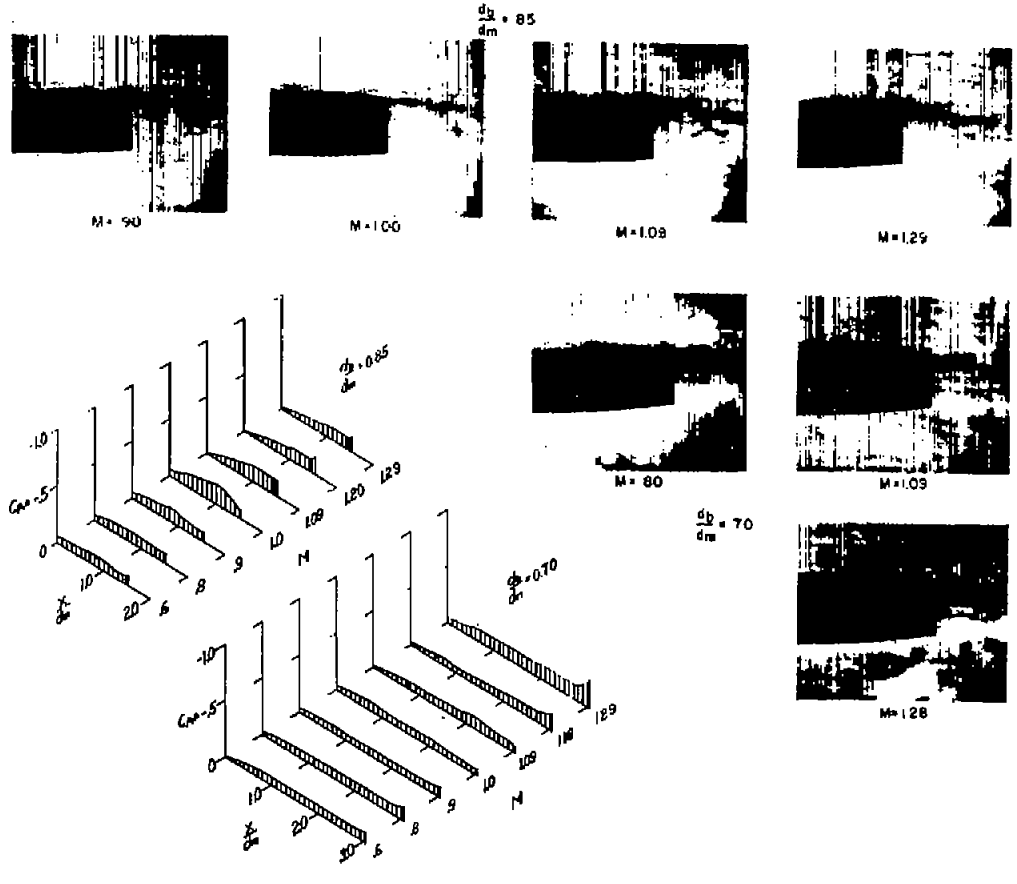

(c) Circular-arc afterbody; $\beta = 5.6^\circ$. L-93610.1

Figure 5.- Continued.

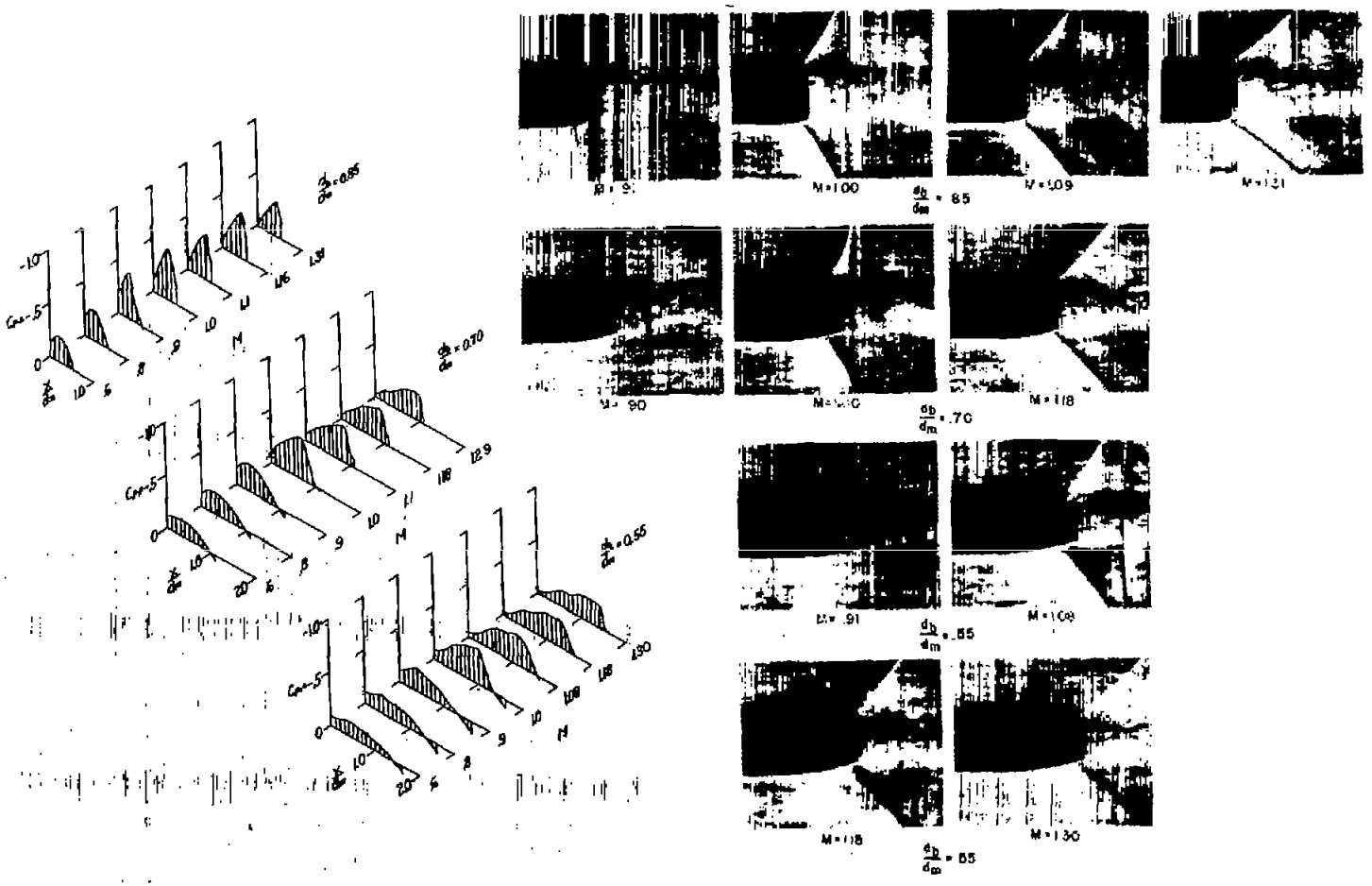

(d) Circular-arc afterbody; $\beta = 16^{\circ}$. L-93609.1

Figure 5.- Concluded.

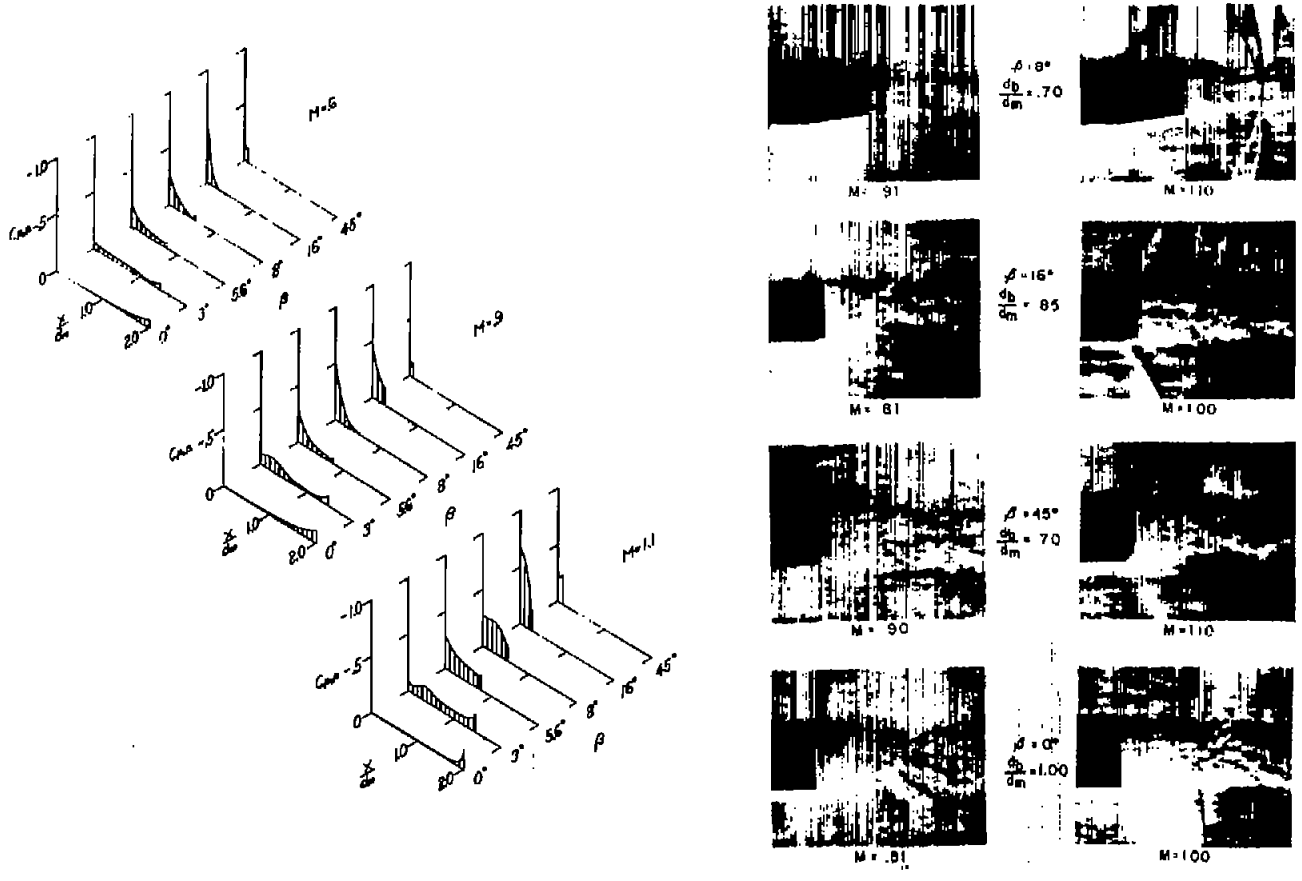

(a) Conical afterbody. L-93607

Figure 6.- Comparison of afterbody pressure-coefficient distributions for different values of boattail angle at three stream Mach numbers. $d_b/d_m = 0.85$.

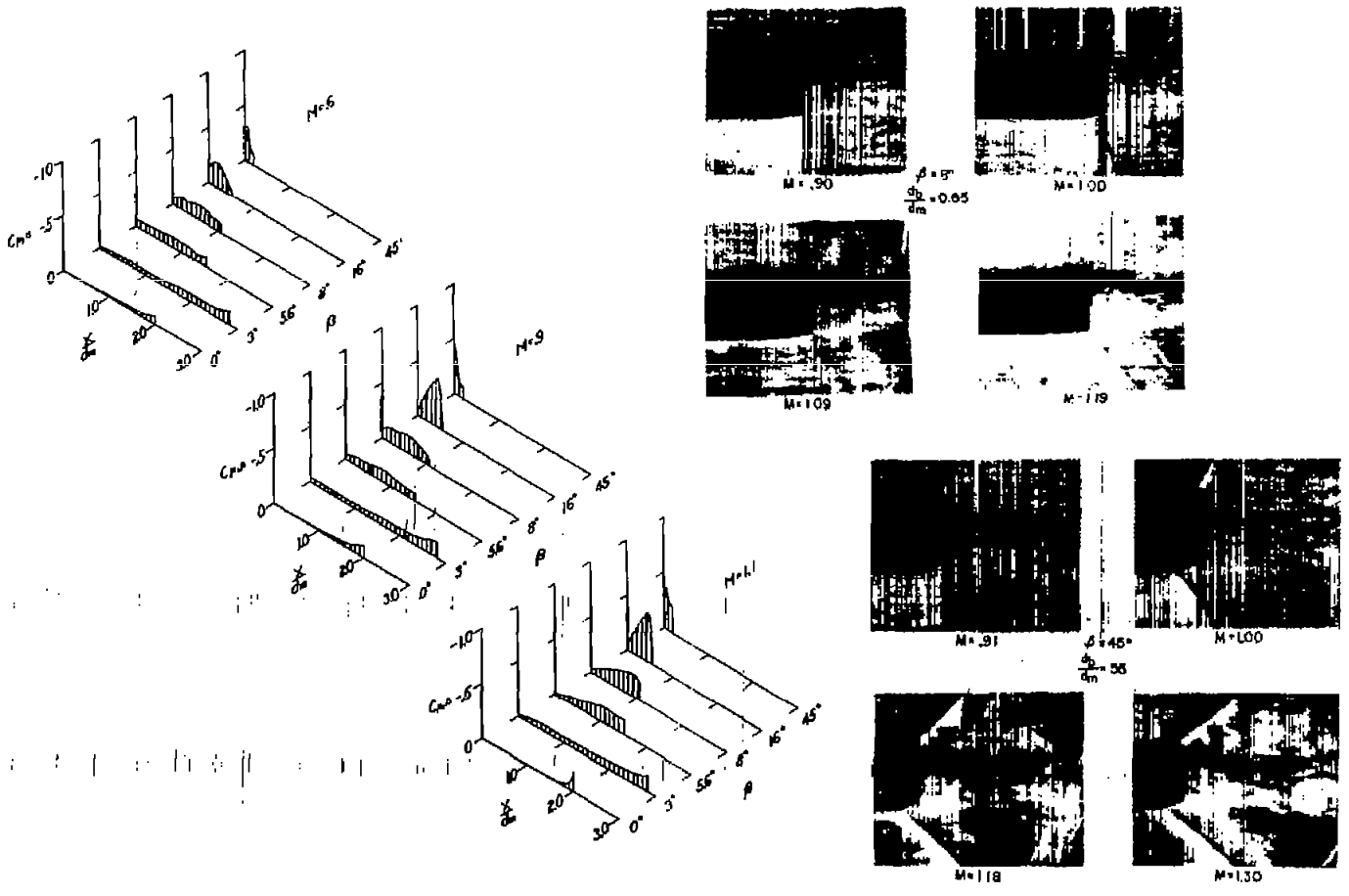

(b) Circular-arc afterbody. L-93608.1

Figure 6.- Concluded.

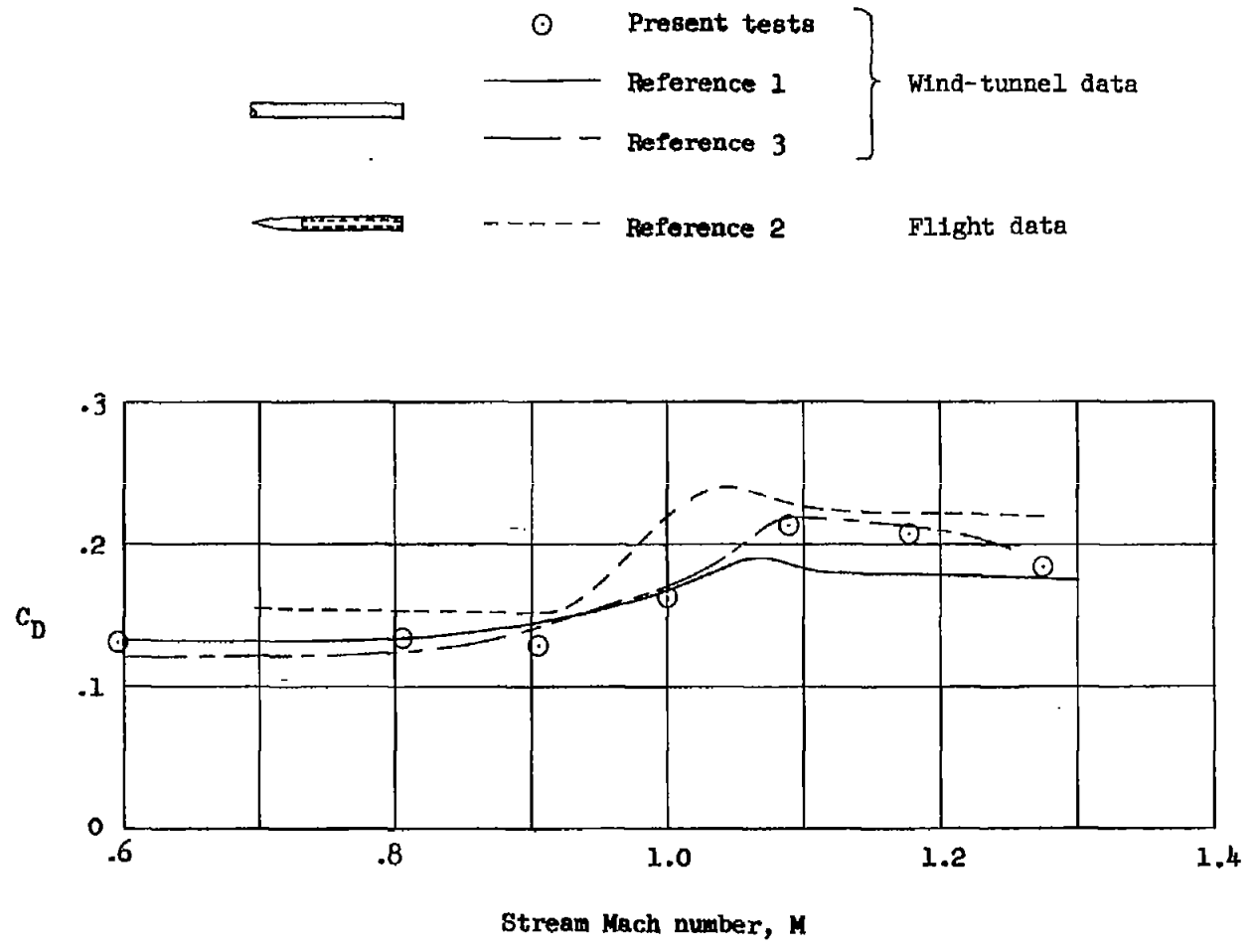

CYLINDRICAL AFTERBODIES

Figure 7.- Comparison of cylindrical afterbody base-drag coefficients from several sources.

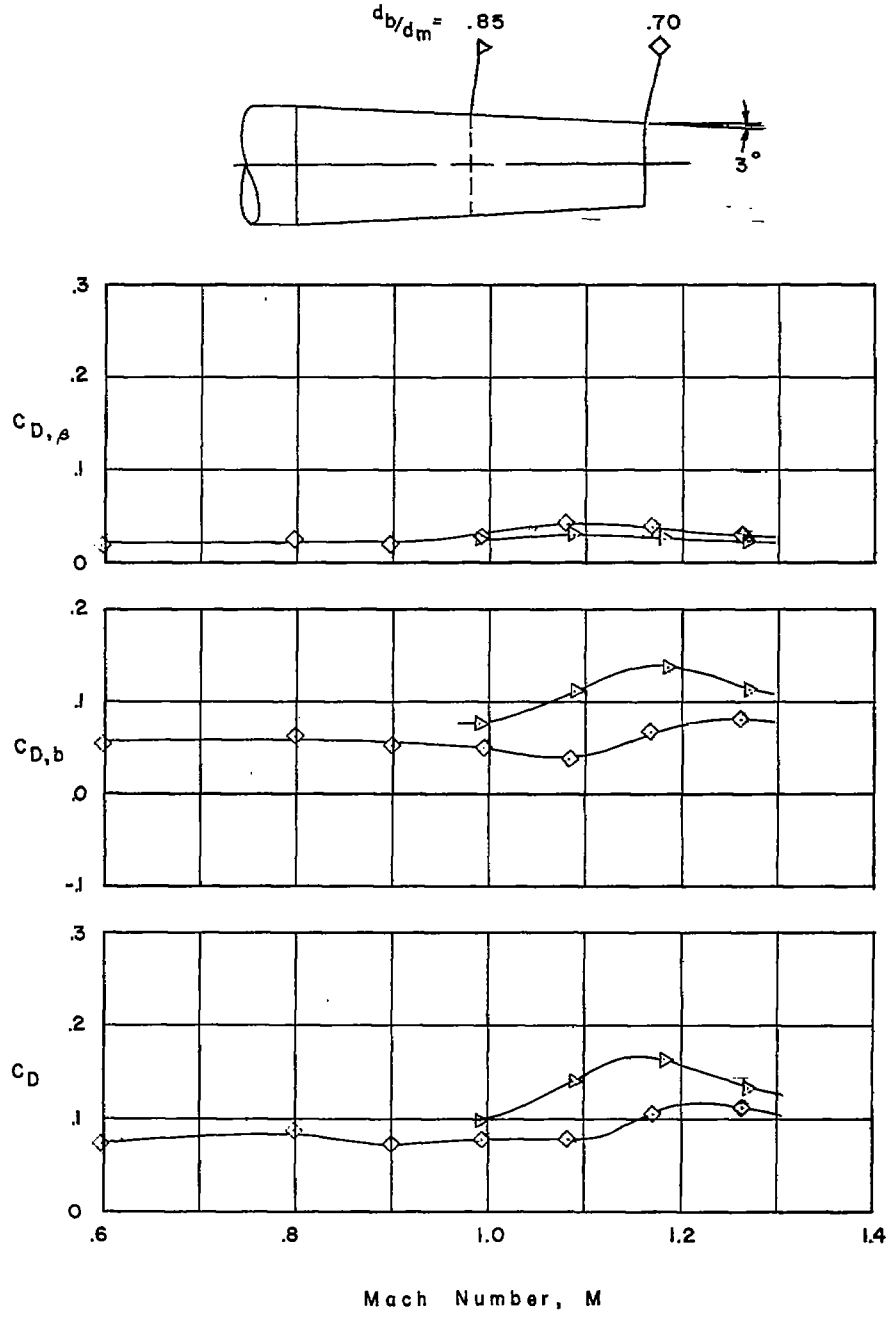

(a) 3° conical afterbody.

Figure 8.- Variation of boattail-, base-, and total-drag coefficients with free-stream Mach number.

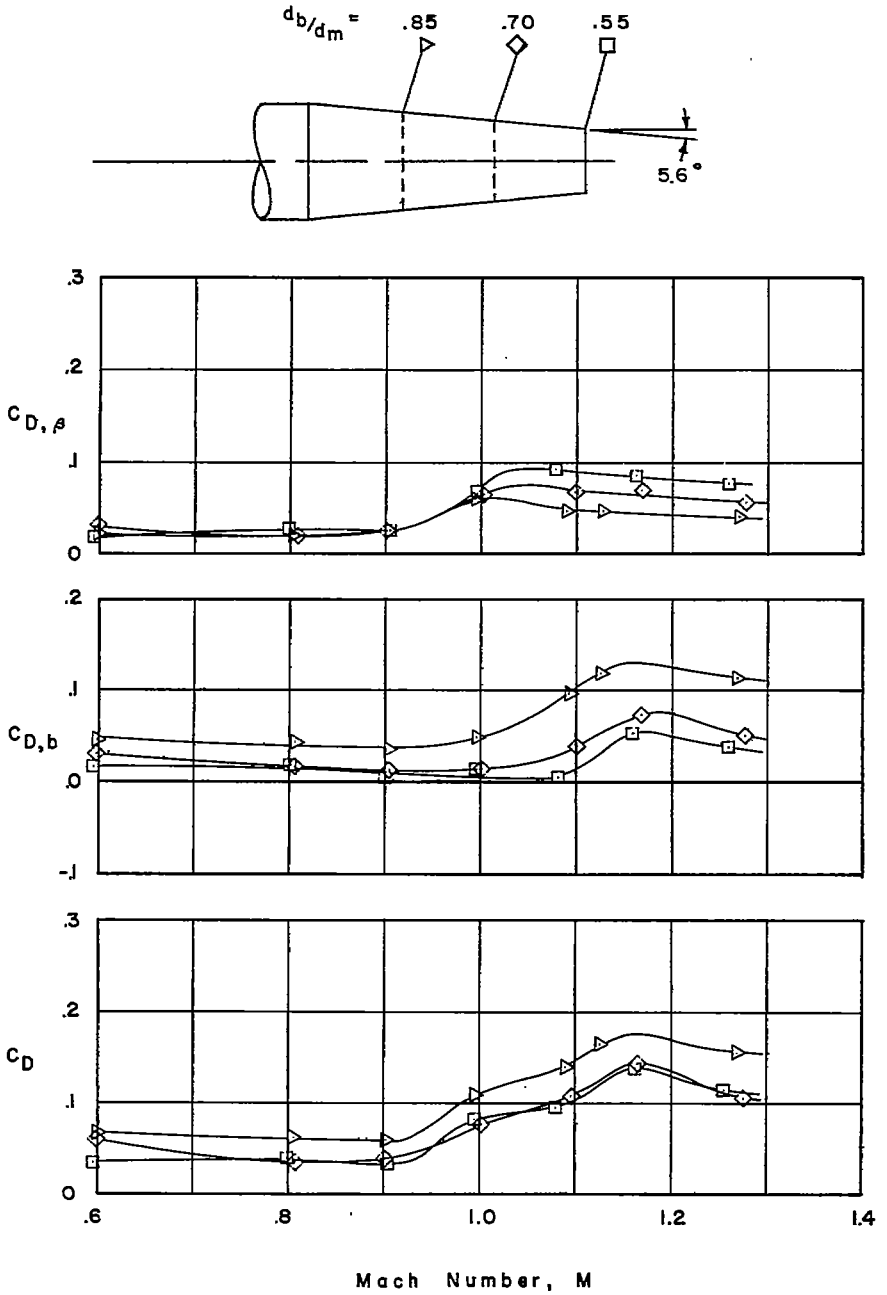

(b) 5.6° conical afterbody.

Figure 8.- Continued.

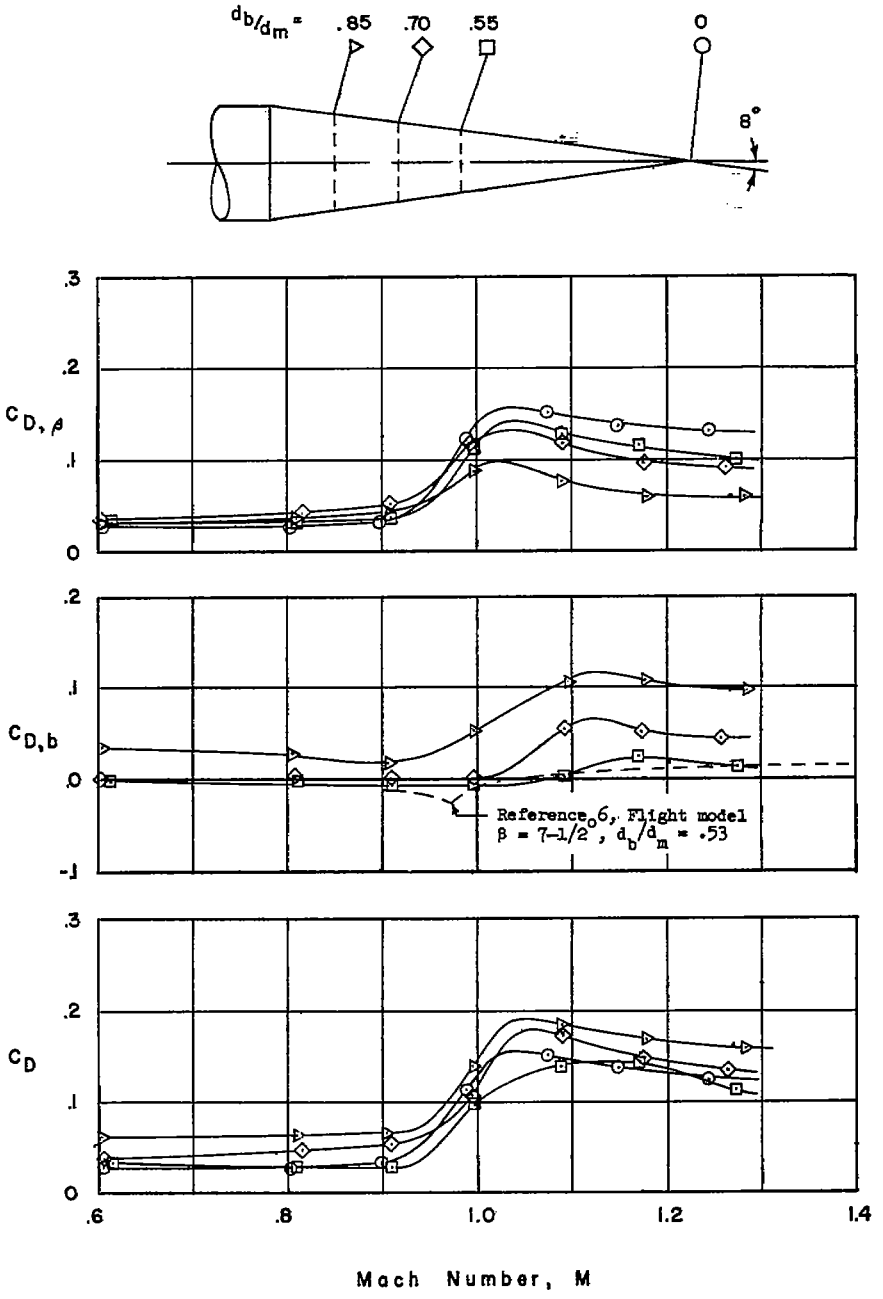

(c) 8° conical afterbody.

Figure 8.- Continued.

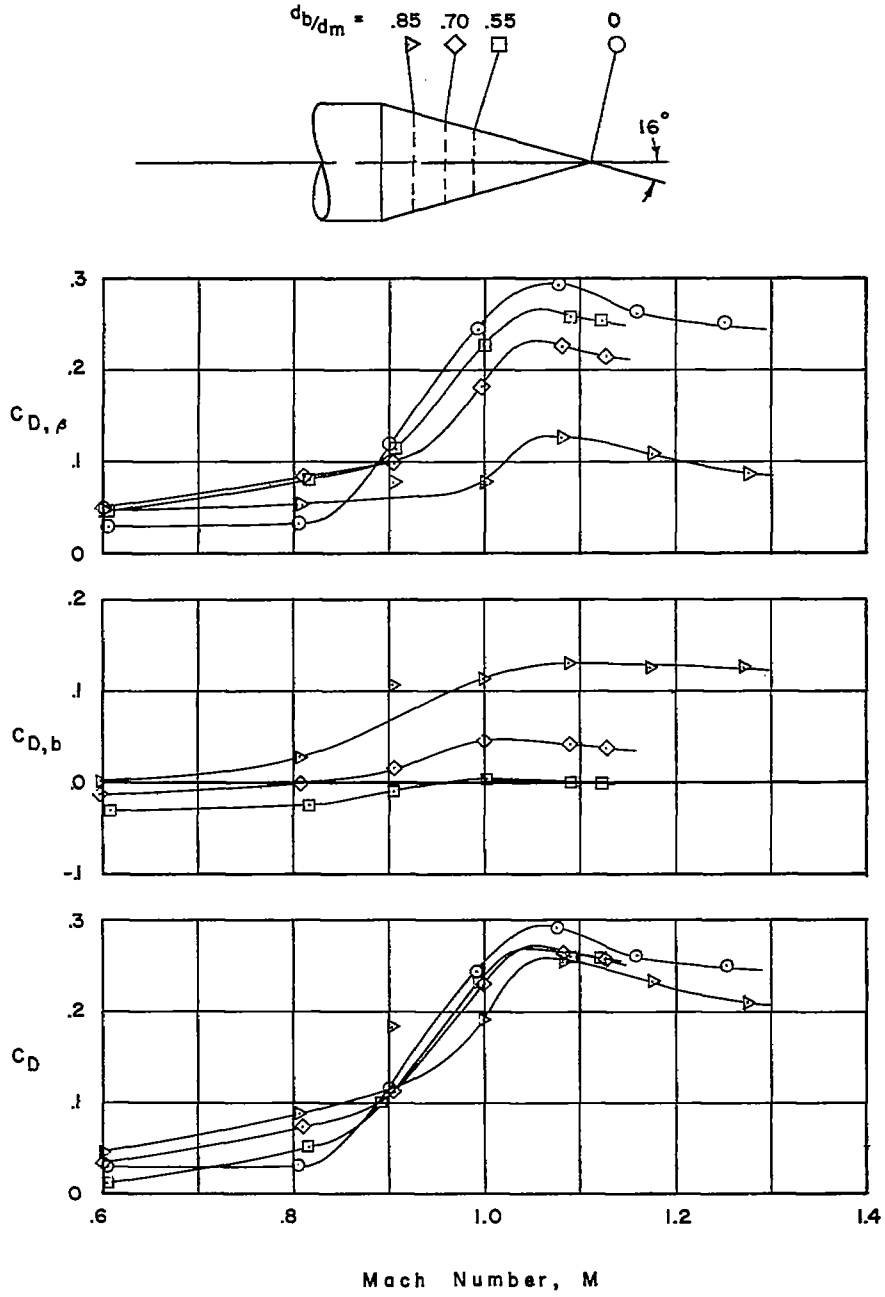

(d) 16° conical afterbody.

Figure 8.- Continued.

[redacted]

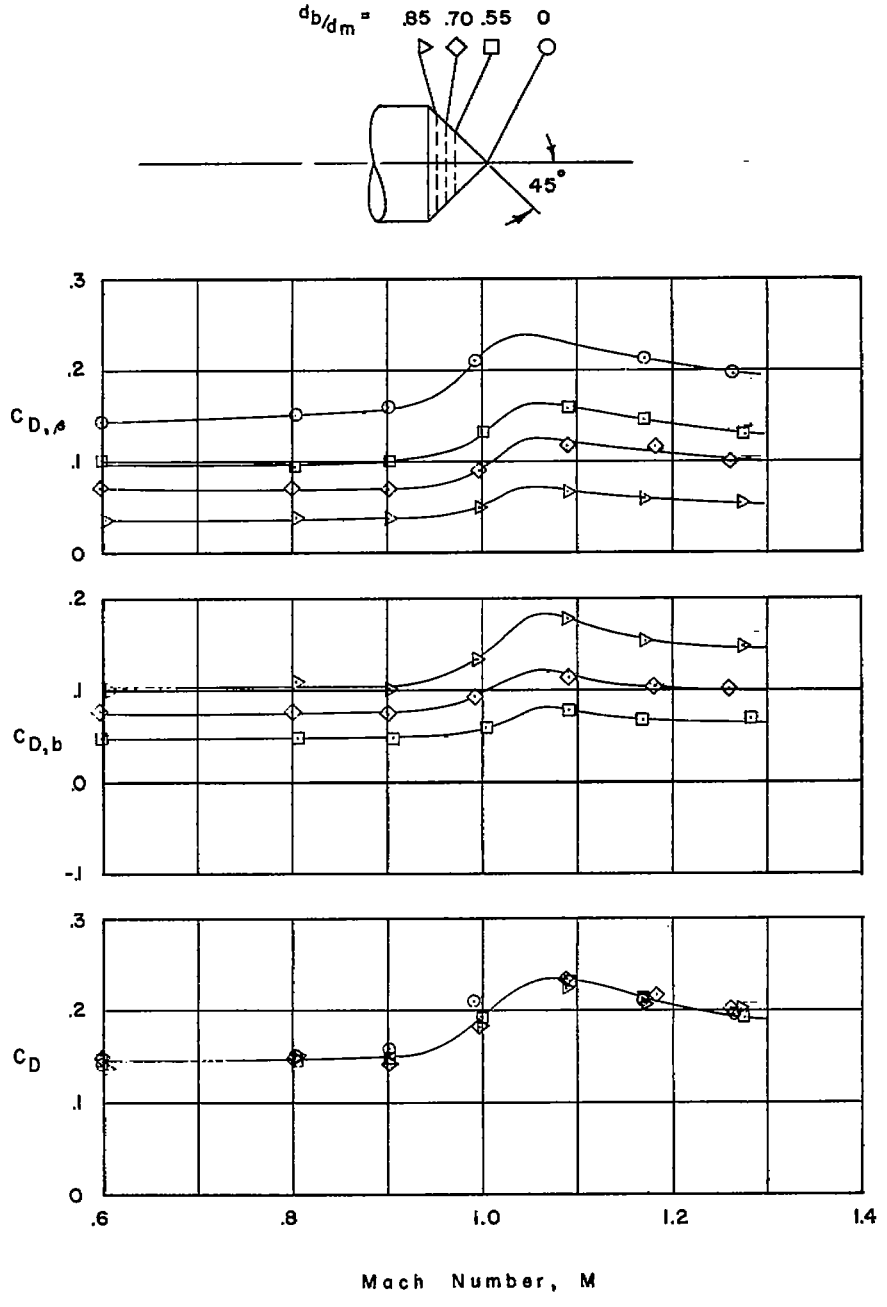

(e) 45° conical afterbody.

Figure 8.- Continued.

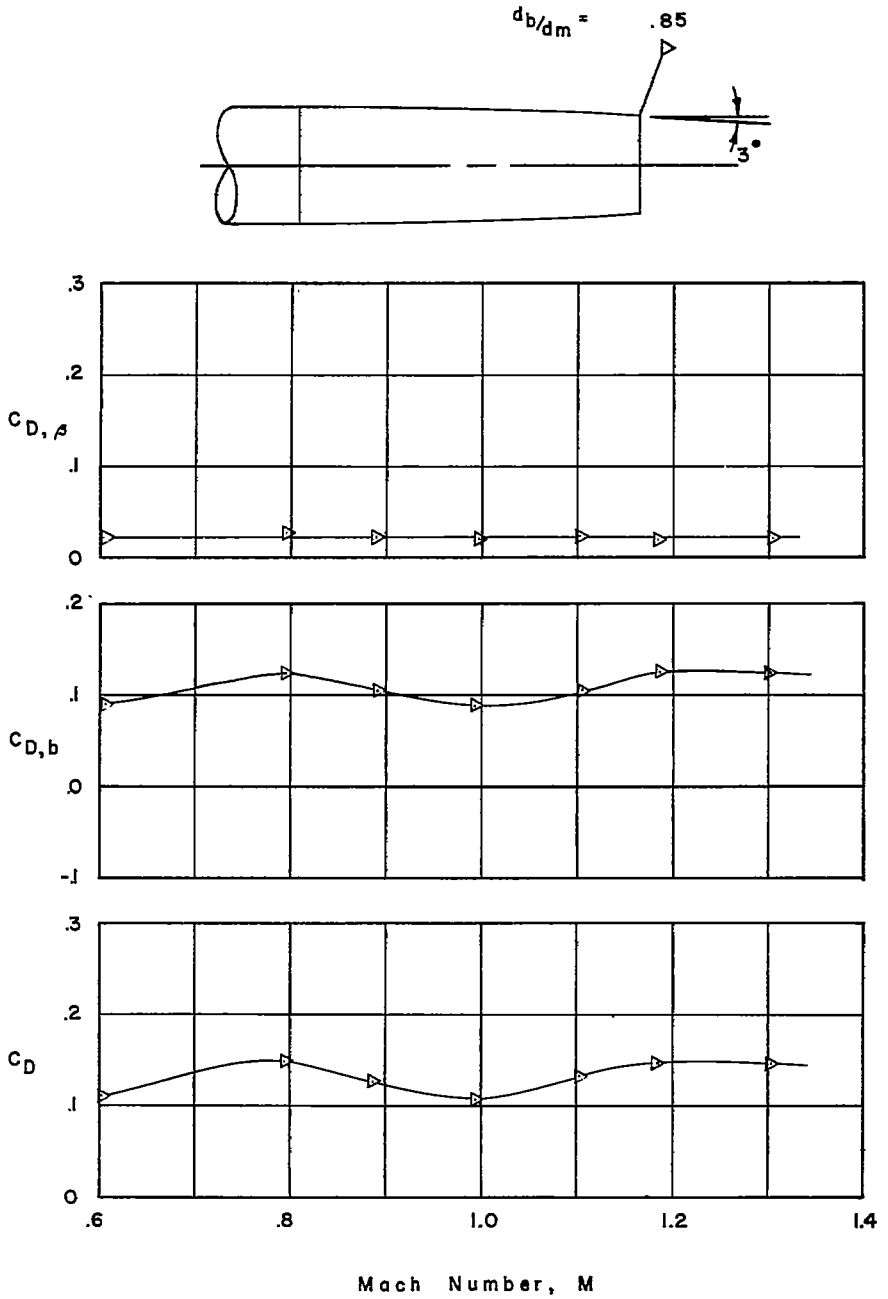

(f) 3° circular-arc afterbody.

Figure 8.- Continued.

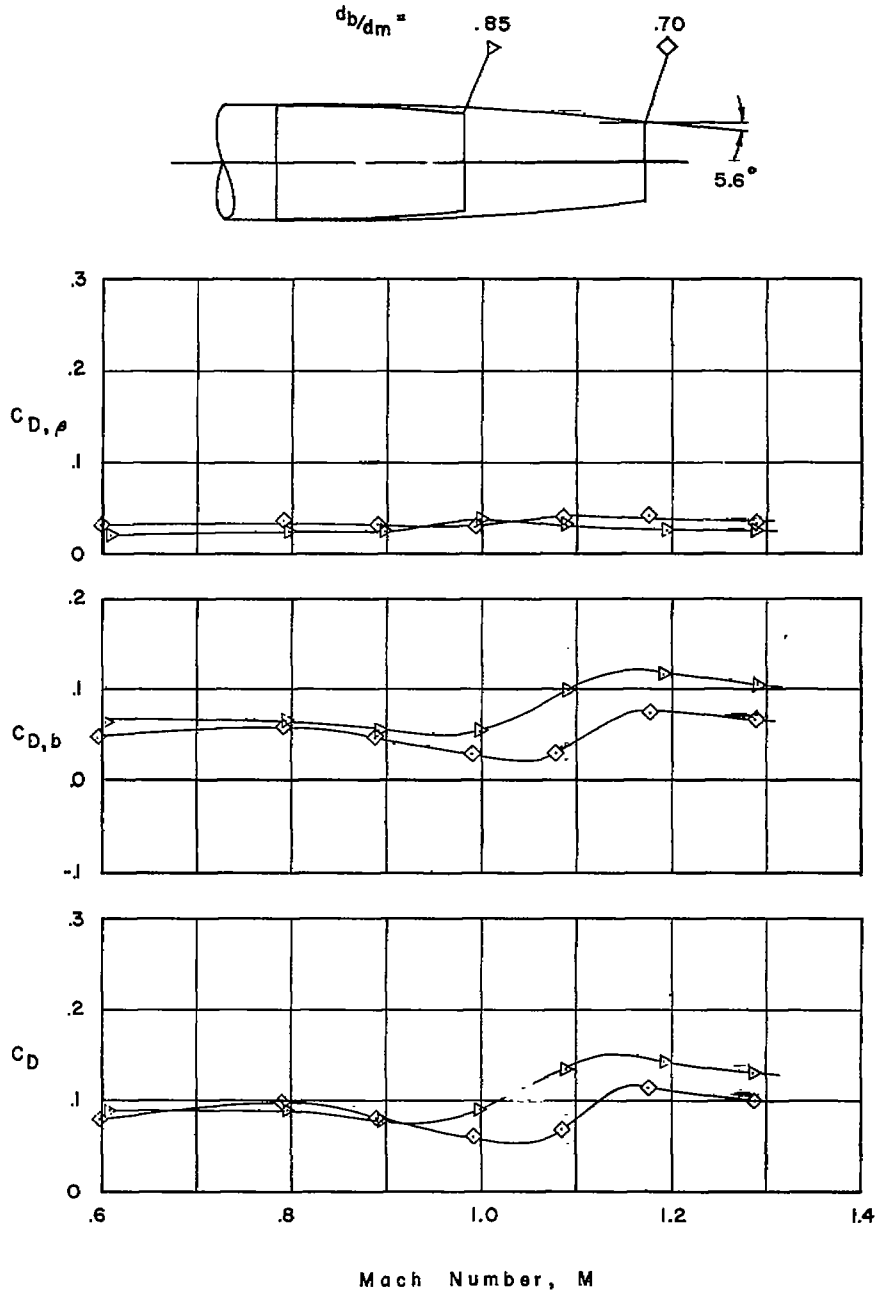

(g) 5.6° circular-arc afterbody.

Figure 8.- Continued.

[redacted]

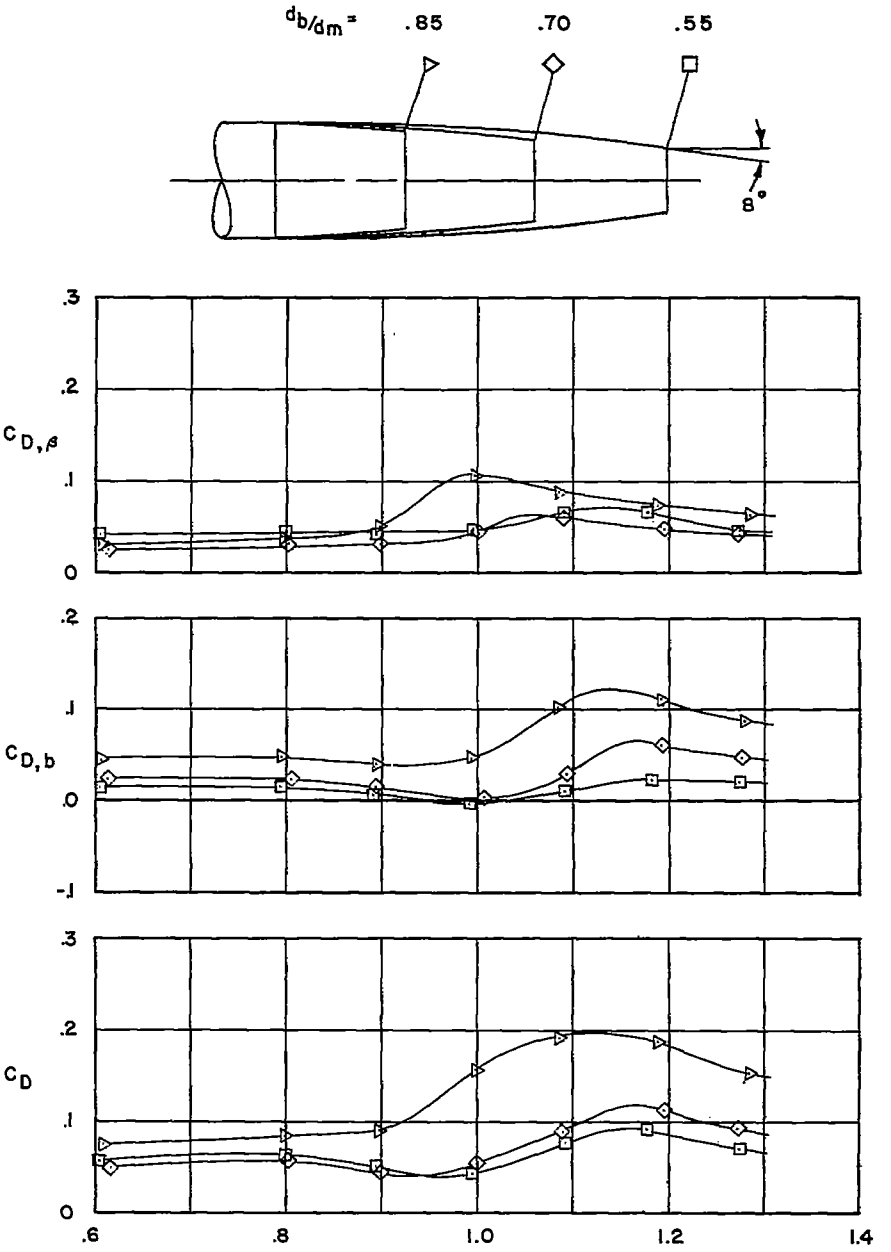

(h) 8° circular-arc afterbody.

Figure 8.- Continued.

[redacted]

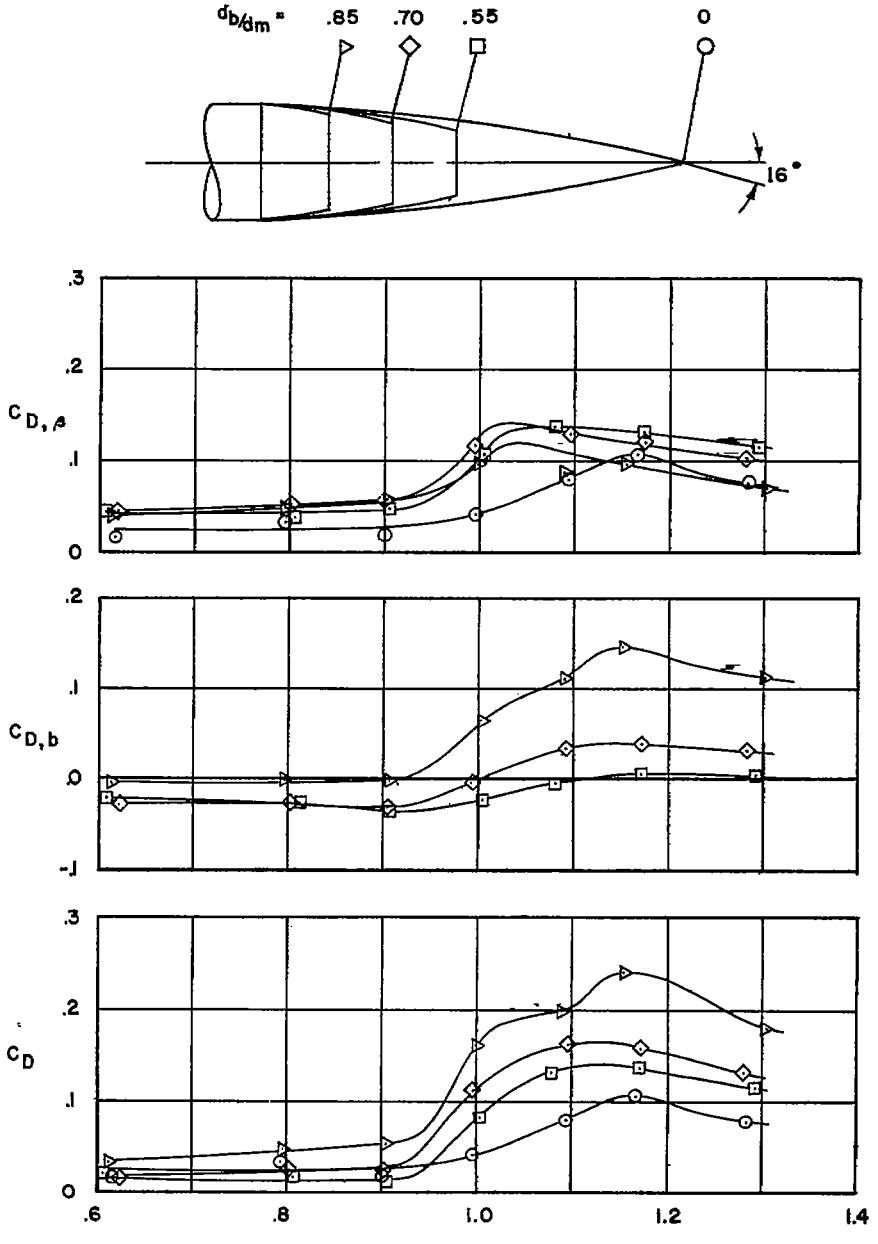

(i) 16° circular-arc afterbody.

Figure 8.- Continued.

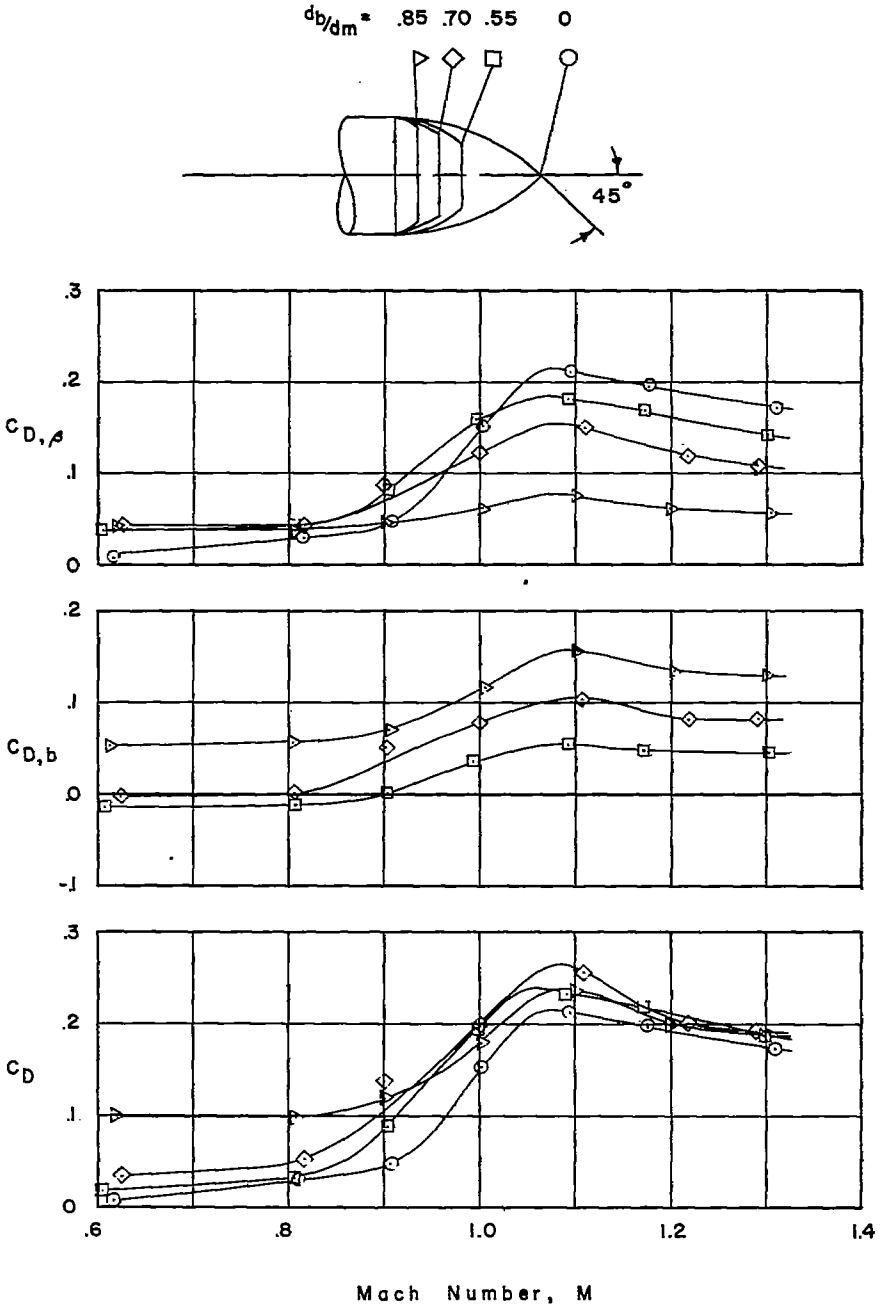

(j) 45° circular-arc afterbody.

Figure 8.- Concluded.

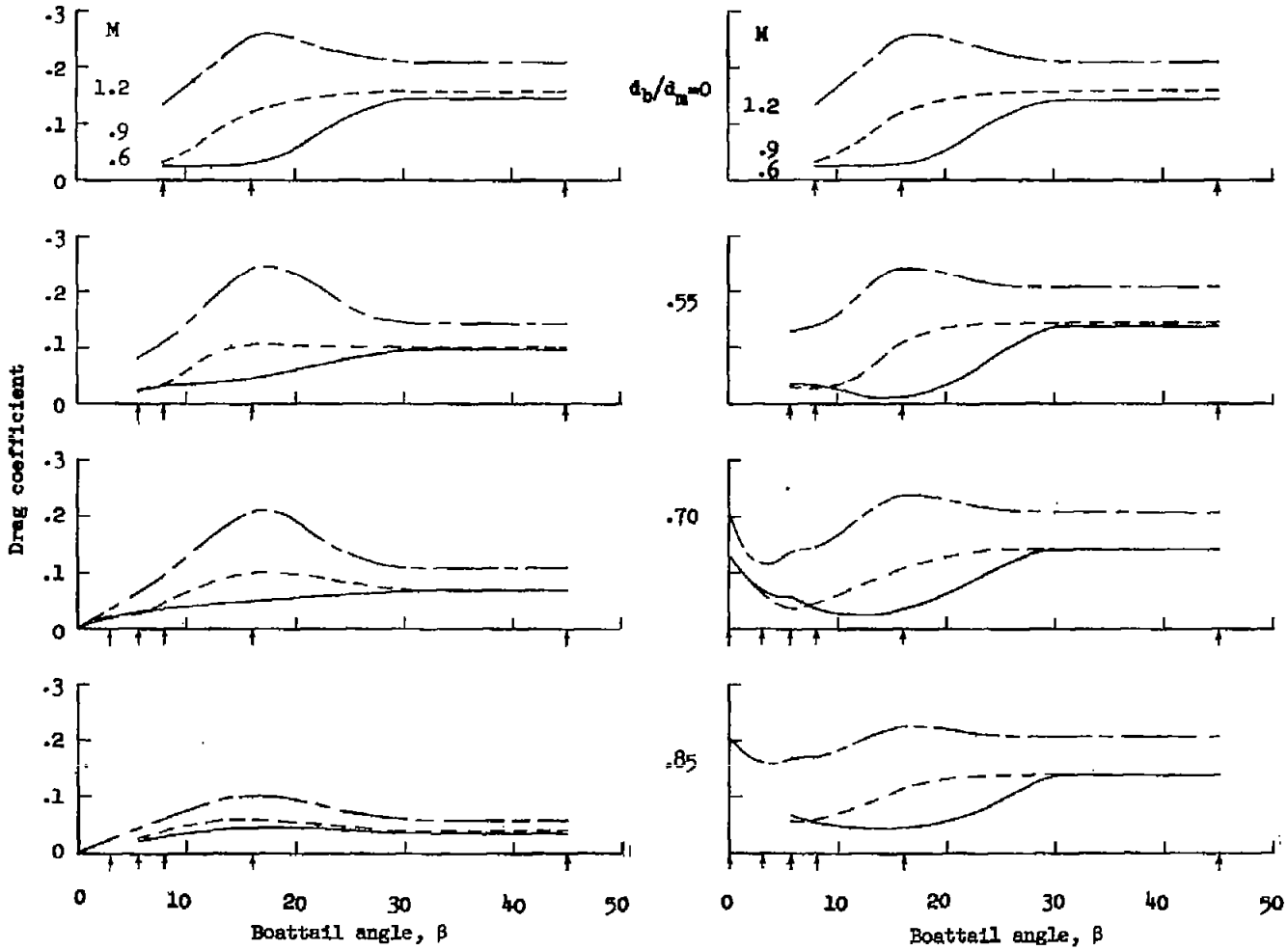

(a) Boattail-drag coefficient.

(b) Total-drag coefficient.

Figure 9.- Variation of boattail- and total-drag coefficients with boattail angle for conical afterbodies. Arrows indicate test points.

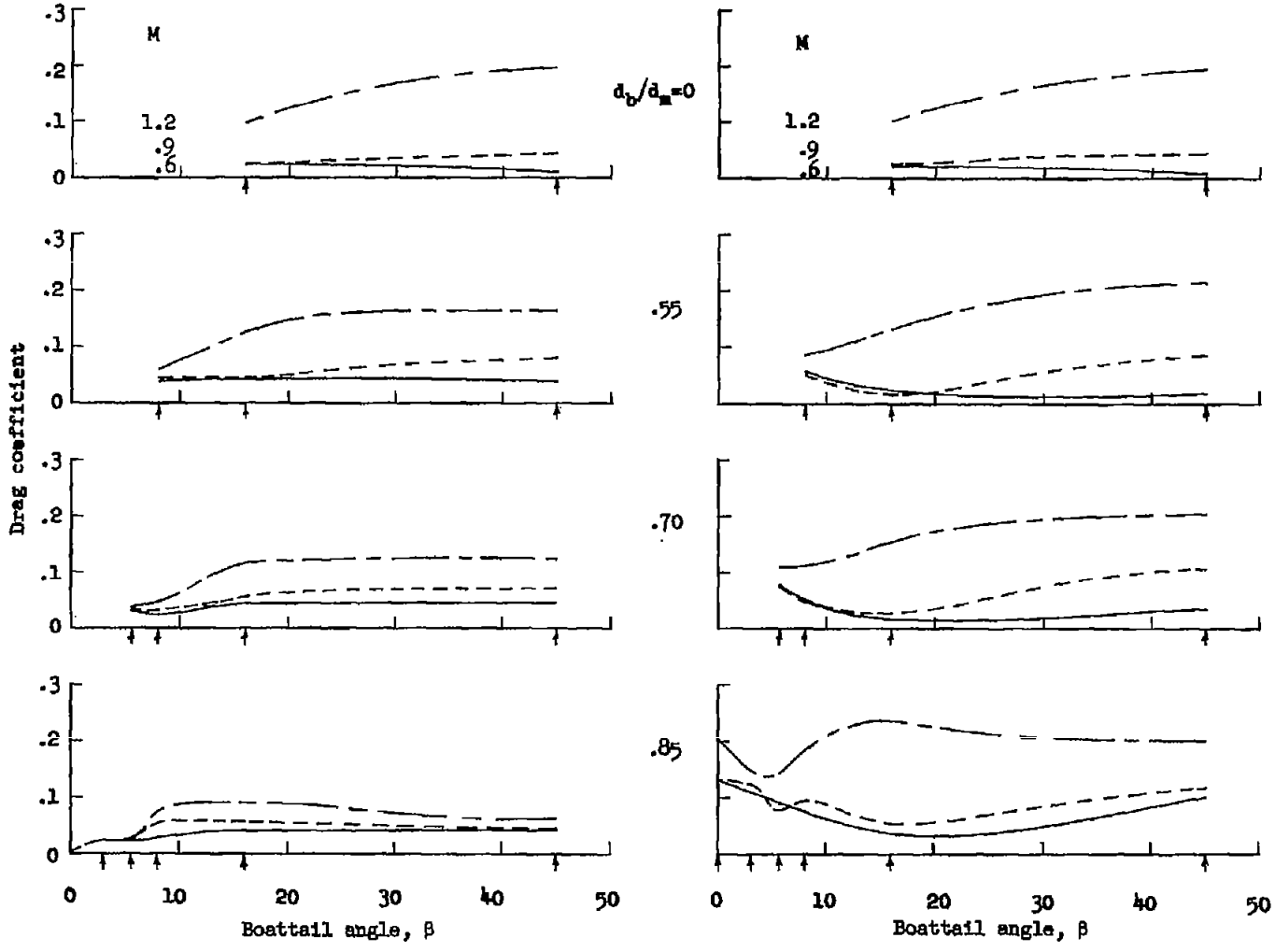

(a) Boattail-drag coefficient.

(b) Total-drag coefficient.

Figure 10.- Variation of boattail- and total-drag coefficients with boattail angle for circular-arc afterbodies. Arrows indicate test points.

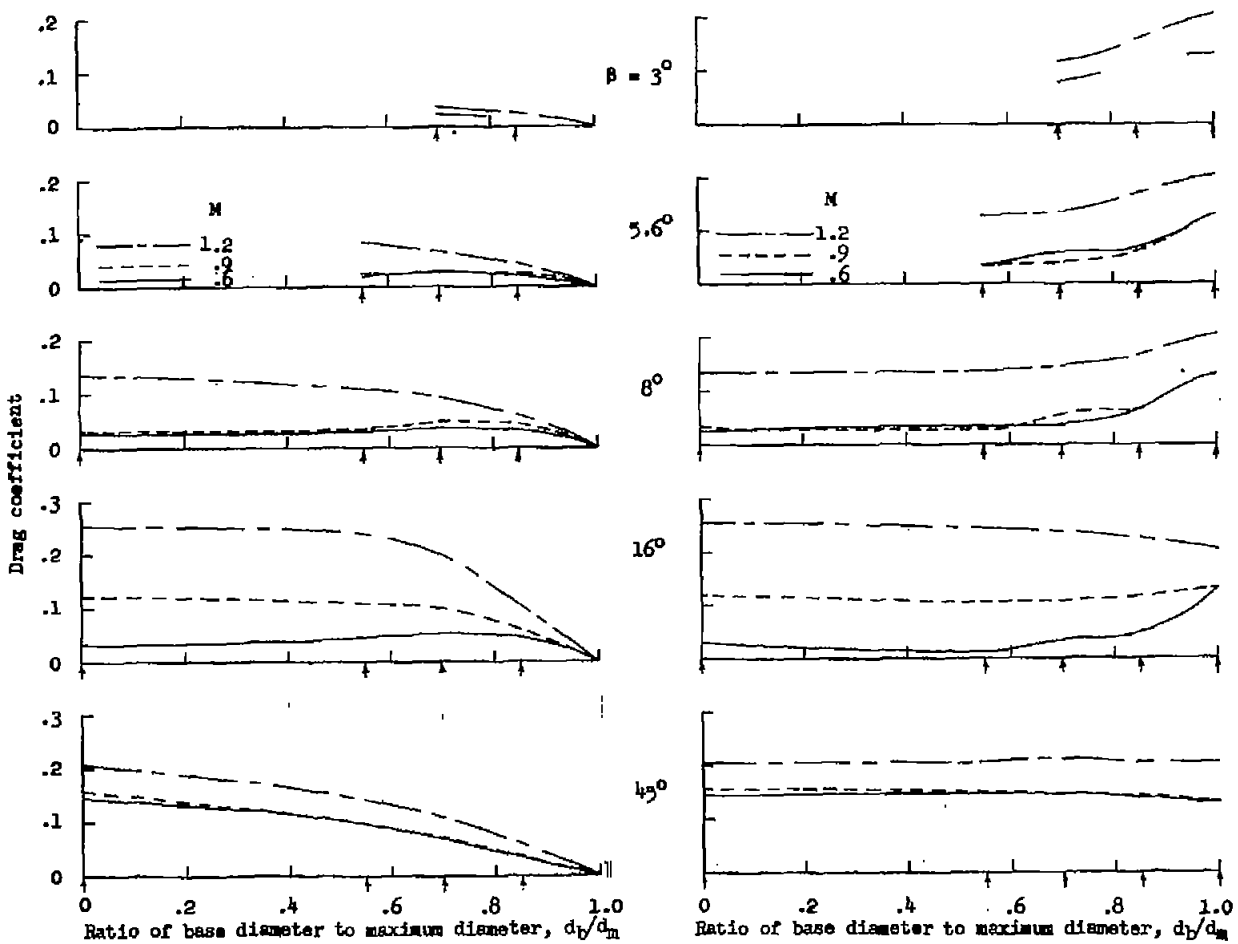

(a) Boattail-drag coefficient.

(b) Total-drag coefficient.

Figure 11.- Variation of boattail- and total-drag coefficients with ratio of base diameter to maximum diameter for conical afterbodies. Arrows indicate test points.

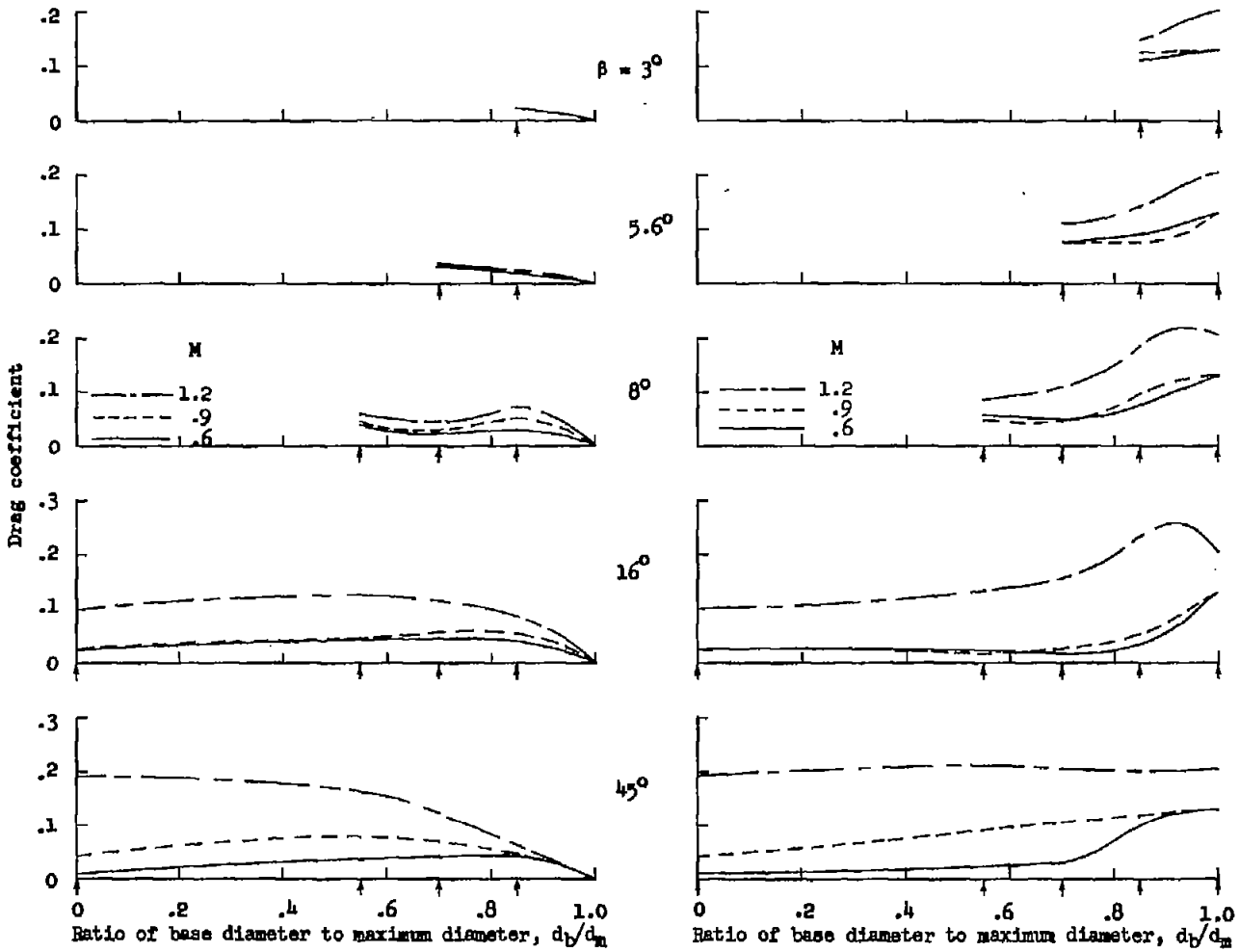

(a) Boattail-drag coefficient.

(b) Total-drag coefficient.

Figure 12.- Variation of boattail- and total-drag coefficients with ratio of base diameter to maximum diameter for circular-arc afterbodies. Arrows indicate test points.

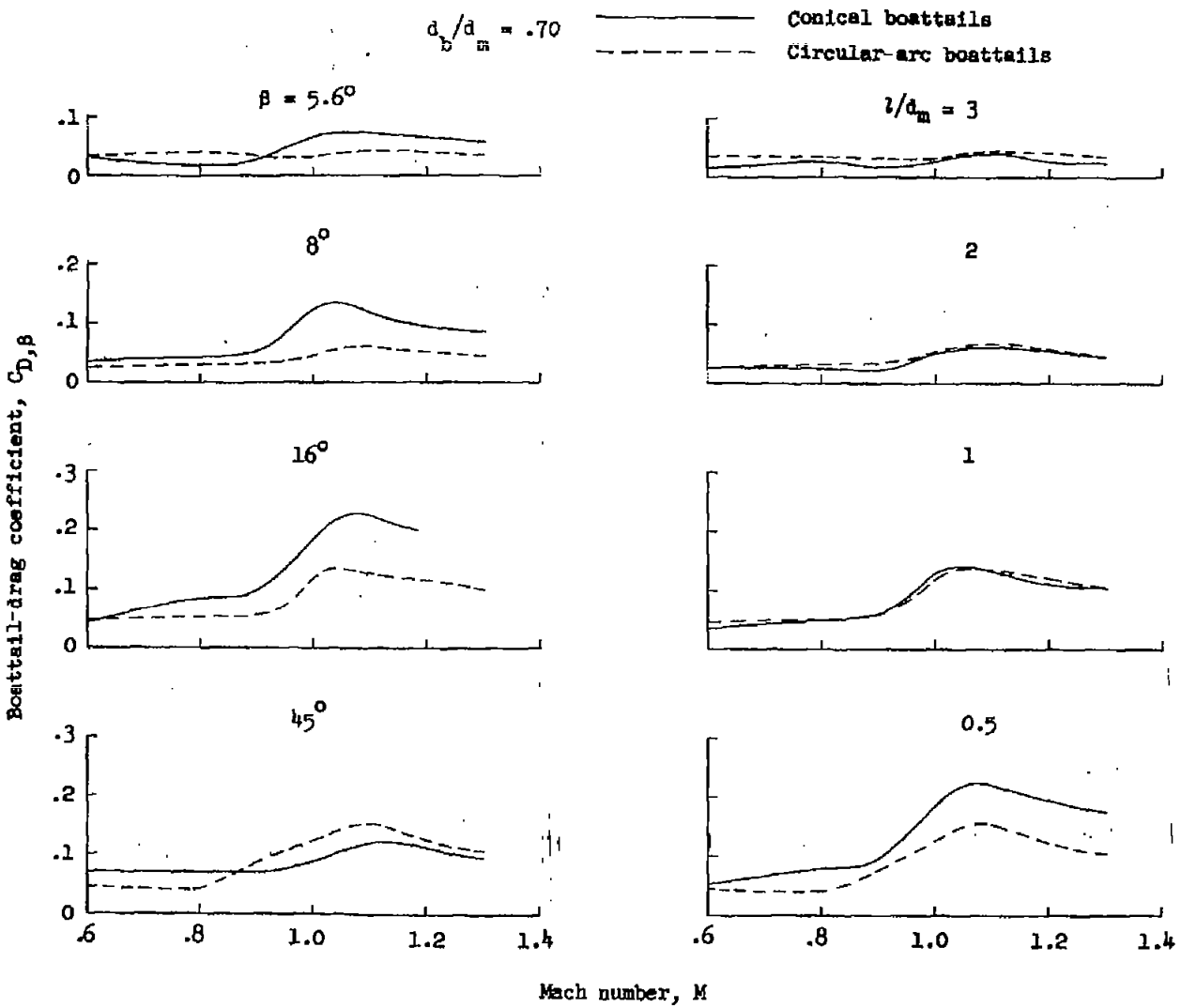

Figure 13.- Boattail-drag comparisons of conical and circular-arc boattailing based on equivalent β and on equivalent fineness ratio for db/dm = 0.70.